ANALYSIS OF ADD/DROP OPTICAL WAVEGUIDE FILTERS WITH PLANAR CAVITY SHAPES

BY

MOHAMMED MISBAHUDDIN

January 2003

ANALYSIS OF ADD/DROP OPTICAL WAVEGUIDE FILTERS WITH PLANAR CAVITY SHAPES

BY

MOHAMMED MISBAHUDDIN

A Thesis Presented to the
DEANSHIP OF GRADUATE STUDIES

KING FAHD UNIVERSITY OF PETROLEUM & MINERALS

DHAHRAN, SAUDI ARABIA

In Partial Fulfillment of the
Requirements for the Degree of

MASTER OF SCIENCE

In

ELECTRICAL ENGINEERING

January 2008

KING FAHD UNIVERSITY OF PETROLEUM & MINERALS

DHAHRAN 31261, SAUDI ARABIA

DEANSHIP OF GRADUATE STUDIES

This thesis, written by

MOHAMMED MISBAHUDDIN

under the supervision of his Thesis Advisor and approved by his Thesis Committee, has been presented to and accepted by the Dean of Graduate Studies, in partial fulfillment of the requirements for the degree of

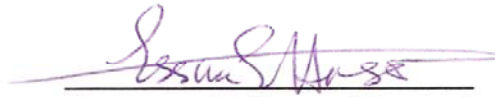**MASTER OF SCIENCE IN ELECTRICAL ENGINEERING**

THESIS COMMITTEE

Dr. Hussain Ali Al - Jamid (Chairman)

Dr. Mohammad M. Al-Sunaidi (Member)

Dr. Essam M. Hassan (Member)

Dr. Ibrahim O. Habiballah
Department Chairman

Dr. Mohammed S. Al-Homoud
Dean of Graduate Studies

Date: 11/2/08

ii

Dedicated to my family

Acknowledgements

In the beginning, I must thank Allah the Almighty and the Most Beneficent and Merciful for His blessings throughout my life in general and in the course of this thesis in particular.

I am indebted to King Fahd University of Petroleum & Minerals (KFUPM) for supporting my M.S. studies and this research work.

I would like to pay a high tribute to my thesis advisor Dr. Hussain A. Al-Jamid for his invaluable guidance and constant help throughout this thesis work. My thesis's quality is a result of the many tiring hours he has spent in helping to refine it. His appreciation and words of encouragement gave a new life to my efforts in hard times. I am always obliged to him for his friendly attitude and endless patients with me.

I would also like to express my deep appreciation to my committee members, Dr. Mohammad M. Al-Sunaidi and Dr. Essam M. Hassan, for their help and encouragement. Their suggestions and critiques were most appreciated.

My acknowledgement also goes to Dr. Ibrahim O. Habiballah, Chairman Electrical Engineering Department for his support.

All I have achieved could not have been possible without the undying love and support from my great family. They gave me the strength and confidence to reach as high as I could both academically and spiritually. They were always there when I needed them and they always had kind and encouraging words throughout my life. Thanks to them.

I am grateful to all my friends specially Mohammed Sameer and Mohammed Abdul Ghani whose company made my stay at KFUPM memorable. Special thanks to Mr. Mohammed Abdul Majid for his encouragement and support.

Table of Contents

vii

List of Figures

xiv

Nomenclature

English Symbols

E   electric field vector, volts/meter

H   magnetic field vector, amperes/meter

N   diagonal matrix of refractive-index squared at mesh grids

I   identity matrix

Q   matrix of eigen-value equation

n   refractive index

k_0 free space wave number, radians/meter

Δx mesh size, meter

j $\sqrt{-1}$

t   time, sec

Greek Symbols

ψ general field component of the **E** or **H** field

Ψ general field component of the **E** or **H** sampled field, column vector

ε_0 free space permittivity, $4\pi \cdot 10^{-7}$ Vs/Am

ε_r	relative permittivity
μ_0	free space permeability, $8.8541\cdot10^{-12}$ As/Vm
μ_r	relative permeability
$\omega = 2\pi f$	angular frequency, rad/sec
α_m	mth modal field coefficient
β	propagation constant, radians/meter
λ	wavelength, meter
∇	nabla operator, $\frac{\partial}{\partial x}\hat{a}_x + \frac{\partial}{\partial y}\hat{a}_y + \frac{\partial}{\partial z}\hat{a}_z$
∇^2	Laplace operator, $\frac{\partial^2}{\partial x^2} + \frac{\partial^2}{\partial y^2} + \frac{\partial^2}{\partial z^2}$

Abbreviations

TE	Transverse Electric
TM	Transverse Magnetic
MOL	Method of Lines
PML	Perfectly Matched Layer
BPM	Beam Propagation Method
ABC	Absorbing Boundary Condition
WDM	Wavelength Division Multiplexing
n_{eff}	Modal Effective Index
λ_B	Bragg Wavelength

Re	Real part of a complex number
Im	Imaginary part of a complex number

Subscripts

A_x, A_y, A_z	x, y, z components of a vector A
ψ_i, ψ_{i-1}, ψ_{i+1}	sample number of field ψ
$\psi_{i\pm}$, $\psi_{i-1\pm}$, $\psi_{i+1\pm}$	field immediately to the left or to the right of a sample point

Superscript

$\psi^{(1)}$	first derivative of ψ
$\psi^{(2)}$	second derivative of ψ
$\psi^{(3)}$	third derivative of ψ
$\psi^{(4)}$	fourth derivative of ψ
$\psi^{(5)}$	fifth derivative of ψ
$\psi^{(6)}$	sixth derivative of ψ
A^*	complex conjugate of A

THESIS ABSTRACT

Name: MOHAMMED MISBAHUDDIN

Title: ANALYSIS OF ADD/DROP OPTICAL WAVEGUIDE FILTERS WITH

PLANAR CAVITY SHAPES

Degree: MASTER OF SCIENCE

Major Field: ELECTRICAL ENGINEERING

Date of Degree: JANUARY 2008

In this thesis work, the filtering and coupling performance of an add/drop filter is analyzed. The basic add/drop filter which has been considered in this thesis consists of two identical and parallel single mode slab waveguides, coupled by a resonant cavity of a planar shape. A number of planar cavity shapes were considered. This includes, for example, the rectangular, the bow-tie, the hexagonal and the parallelogram shaped cavities. The Method of Lines (MOL) using the Layer by Layer Algorithm has been applied to model these add/drop filters.

Keywords: Method of Lines (MOL), Add/Drop Filter, The Layer by Layer Algorithm.

Master of Science Degree

King Fahd University of Petroleum & Minerals, Dhahran.

January 2008

ملخص الأطروحة (الرسالة)

الإسم: محمد مصباح الدين

العنوان: تحليل مرشح الإضافة و الطرح البصري للموجة المرشدة بأشكال تجويفية

الدرجة: ماجستير علوم

التخصص الرئيس: هندسة كهربائية

تاريخ الرسالة: يناير ٢٠٠٨م

لقد تم تحليل مرشح الإضافة و الطرح لأداء الرشح و التآلف في هذه الرسالة. يتألف مرشح الإضافة و الطرح الذي تم أخذه بالإعتبار في هذه الرسالة من موجتين ارشاديتين متماثلتين و متوازيتين بتناغم انفرادي، مقرونة مع تجويف رنيني لشكل مستوي. لقد تمت دراسة عدد من أشكال التجويف المستوي هنا. و هذا يشمل، على سبيل المثال الأشكال التجويفية على شكل المستطيل، القوسي، السداسي و المتوازي الأضلاع. لقد تم تطبيق النمط الخطي (MOL) باستعمال طبقة تلو طبقة ليتطابق مع نمط هذه المرشحات للإضافة و الطرح.

المصطلحات الرئيسية: النمط الخطي (MOL)، مرشح إضافة و طرح، الحساب الطبقي

درجة الماجستير في العلوم

جامعة الملك فهد للبترول و المعادن ـ الظهران

يناير ٢٠٠٨

Chapter 1

Introduction

1.1 Integrated Optics

Integrated Optics (IO) is the technology concerned with the design and fabrication of Optical Integrated Circuits (OIC). OICs consist of various miniature optical components placed on a dielectric substrate and connected via waveguides. They are capable of performing functions such as modulation, switching, filtering, signal generation and processing. The concept of IO was first proposed by S. E. Miller of Bell labs in 1969 [1, 2].

In the OIC, the signal is carried by means of light confined in thin film waveguides that are deposited on the surface or buried inside a substrate. Glasses, dielectric crystals and semiconductors can be used as substrate materials. The functions that can be realized depend on the type of substrate used. The most fundamental building block of an OIC is the waveguide. The basic requirements of a waveguide are that it should be transparent to the wavelength of interest and have a refractive index higher than that of the medium in which it is embedded. Then the light waves can propagate over a distance with considerably low transmission losses due to the phenomena of Total Internal Reflection (TIR).

The advantages of OIC over other technologies are compact size, light weight, low power requirements, low transmission loss, large bandwidth, immunity to electromagnetic interference, low cost, etc. [3]. Due to the high information carrying capacity, OICs are extremely useful and have many applications in the field of telecommunication. Optical fiber communication is one of the most promising applications of IO. The optical fibers have extremely large transmission rate and provide a very secure communication [4]. In recent years there has been an enormous increase in the bandwidth requirements for telecommunication and data communication systems, mostly due to the growth of the internet. Advances in IO components, which are the foundation of such systems, have enabled systems to meet these ever-increasing demands.

1.2 Add/Drop Filters

The add/drop filter is an optical wavelength filter that can extract one wavelength from a group of wavelengths and also add a specific wavelength to the group. One type of add/drop filter consists of a resonant cavity imbedded between two parallel and identical waveguides. When an optical signal that operates away from resonance is launched in one of the waveguides, it will exit through the other side of that waveguide. However, at resonance, the optical signal will be coupled to the other waveguide and optical power will exit the device through one of the terminals of this waveguide.

Resonant cavities can be of different shapes and sizes. The shape and size of the resonant cavity greatly effects the filtering and coupling performance of an add/drop filter. The air gap width between the cavity and waveguides also play a very crucial role in effecting the filtering and

coupling performance of an add/drop filter. The refractive index of the resonant cavity is usually equal to that of the waveguides and greater than the surrounding medium.

Add/drop filters can also extract more than one wavelength from a group of wavelengths [5]. Wavelength tunable optical add/drop filters have also been reported in the literature [6], where transmission to the other ports can be tuned to the wavelength of interest. This can be achieved by varying the parameters of the resonant cavity. Tunable wavelength filters with a narrow bandwidth and a wide tuning range are useful for the purpose of selecting one wavelength carrying desired information among the wavelength-division-multiplexed (WDM) signals [7]. Add/drop filters that access one channel of a WDM system without disturbing other channels are very important components for WDM communications [8].

1.3 High Index Contrast IO

High index contrast means that the ratio of the difference between the highest and the lowest refractive index in a device to their sum is of the order of 50% or more. High index contrast allows for strong confinement and ultra-compact devices. The strong confinement can be achieved either by waveguide confinement or by cavity confinement or by a combination of both. In case of cavity confinement, high index contrast allows the realization of cavities with very small size and narrow bandwidth. This is important for low power and high speed operation of filters, modulators, switches, etc. High index contrast can most easily be achieved by using a combination of semiconductor material with a low-index dielectric. In past few years there has been an enormous progress in the field of high index contrast IO [9].

The structures proposed in this thesis work exhibit high index contrast in order to achieve the above mentioned advantages.

1.4 Literature Review and Thesis Research Work

In this thesis, we propose to analyze the filtering and coupling characteristics of add/drop filters that utilize resonant cavities with planar shapes. The add/drop filters to be studied consist of two parallel and identical slab waveguides with an imbedded resonant cavity. A brief literature review of reported add/drop filters will be presented followed by a statement of the proposed research work to be done in this thesis.

1.4.1 Literature Review

Add/drop wavelength filters with resonant cavities of various shapes have been reported in the literature. This includes filters that utilize squared-shaped resonant cavities [10, 11, 12], as shown in Fig.1.1 (a). An add/drop filter that utilize an octagonal resonant cavity (see Fig. 1.1 (b)), has also been previously report [13]. In addition, the hexagonal-shaped resonant cavity shown in Fig 1.1 (c) has been considered [14]. The most commonly used cavity shapes are the circular [10, 15] and the ring-shaped resonant cavities [16, 17], which are respectively shown in Figs. 1.1 (d) and 1.1 (e). An add/drop filter that utilize an elliptically-shaped cavity (see Fig. 1.1

(f)) has also been reported [10]. For all the add/drop filters shown in Fig 1.1, the top waveguide is called the bus and the bottom waveguide is called the receiver.
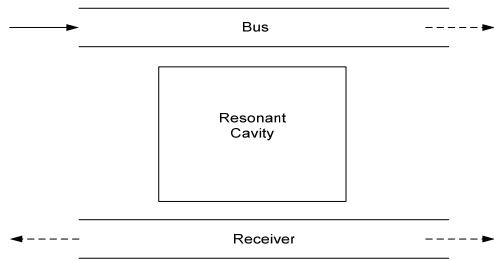
(a) Square Cavity
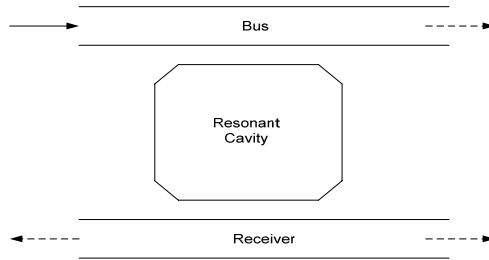
(b) Octagonal Cavity
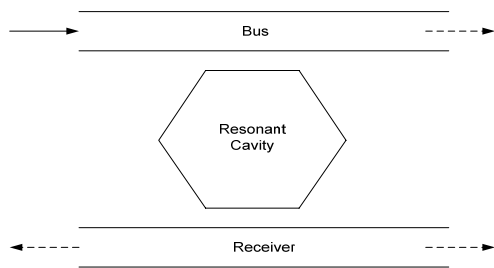
(c) Hexagonal Cavity
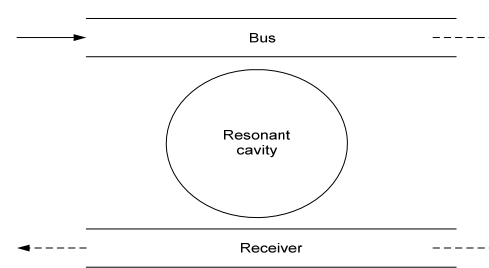
(d) Circular Cavity
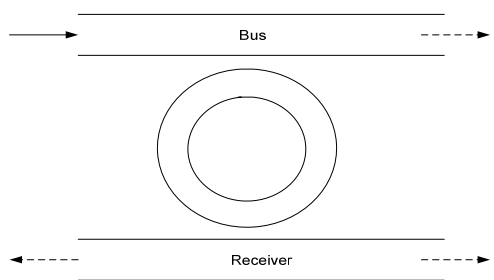
(e) Ring Cavity
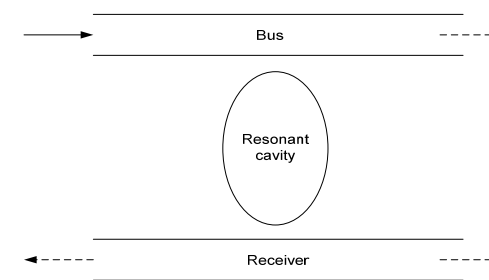
(f) Elliptical Cavity

Figure 1.1: Add/Drop Filters with different Cavity Shapes.

1.4.2 Thesis Work

The proposed work in this thesis consists of the analysis of add/drop filters that utilize resonant cavities that are planar in shape. The structure to be analyzed consists of two identical and parallel single mode slab waveguides that are separated by a sufficiently large distance. This insures isolation of the two parallel slab waveguides. A resonant cavity of a planar shape will be placed between the two isolated slab waveguides. Analysis of the filtering and coupling characteristics will be done by calculating the spectral response of the resulting structure. The proposed add/drop filters will be modeled using the Method of Lines (MOL) in tandem with the Layer by Layer Algorithm.

A number of planar cavity shapes will be considered. This includes, for instance, the rectangular cavity (see Fig. 1.2(a)), the bow-tie shaped cavity (see Fig. 1.2(b)), the hexagonal shaped cavity (see Fig. 1.2(c)) and the parallelogram shaped cavity (see Fig. 1.2(d)). The spectral response, of the add/drop filter with the proposed cavity shapes, will be calculated in order to study the effect of the air gap length g and the width w of these cavities. In the case of the bow-tie and hexagonal cavities, the effect of the angle θ will also be investigated.
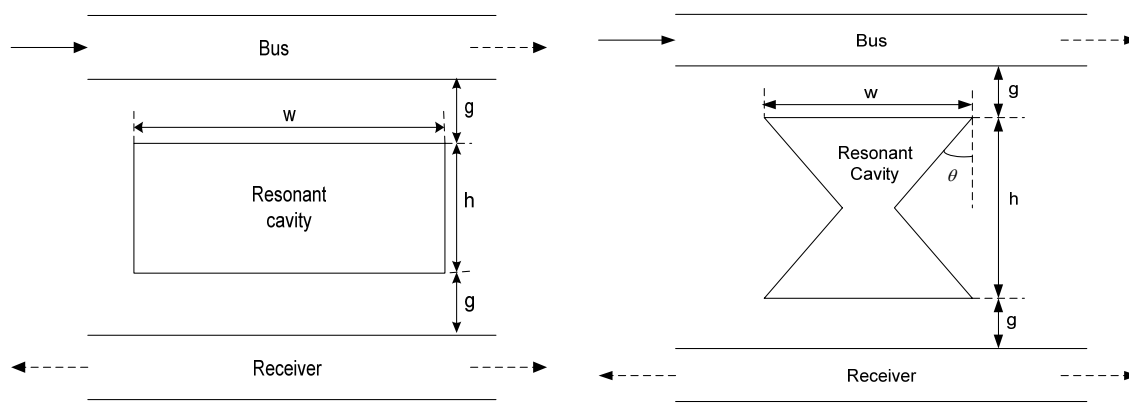
(a) Rectangular Cavity

(b) Bow-tie Shaped Cavity
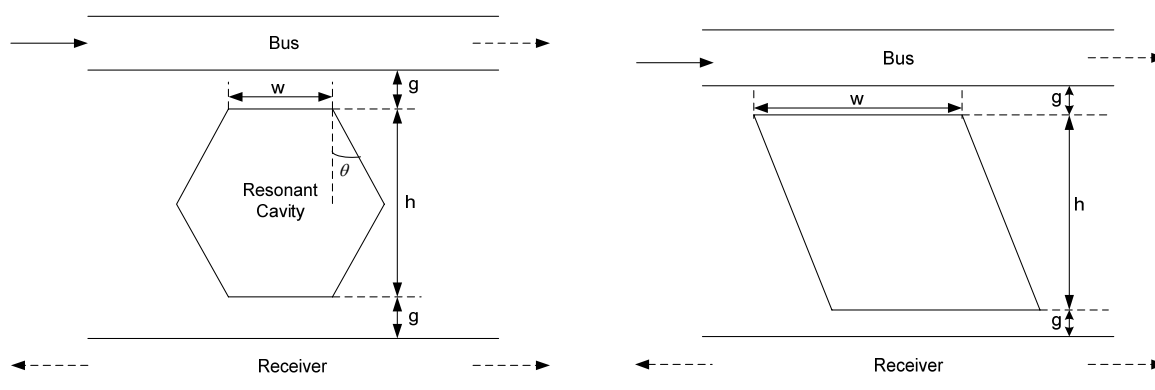
(c) Hexagonal Cavity

(d) Parallelogram Shaped Cavity

Figure 1.2: Proposed Structures

1.5 Organization of the thesis

For the reader to easily follow the progress of the work, this thesis is organized in the following manner. It consists of nine chapters. The first chapter is an introductory chapter which includes introduction to IO and add/drop filters along with a description of the research work to be done in this thesis. The second chapter introduces the basic MOL and describes how the eigenpairs are utilized in the field calculations. Implementation of the Perfectly Matched Layer (PML) absorber is also explained in this chapter. In the third chapter, MOL analysis of longitudinal waveguide discontinuities is presented. The fourth chapter introduces directional coupler and add/drop filters. In the fifth chapter the analysis of add/drop filter with square cavity is presented. The layer by layer algorithm is also introduced in this chapter. Chapters six, seven and eight are devoted to the analysis of add/drop filter with rectangular, bow-tie, hexagonal and parallelogram cavities. The final chapter, chapter nine, summarizes the presented work, concludes and suggests future extension of the thesis work.

Chapter 2

The Method of Lines (MOL)

2.1 Introduction

Various numerical algorithms have been proposed and implemented successfully for the analysis of optical waveguide structures. One of these methods is the MOL [18-30]. It is regarded as a special finite difference method but more effective with respect to accuracy and computational time. It basically involves discretizing a given differential equation in one or two dimensions while using analytical solution in the remaining direction. It has the merits of both the finite difference method and analytical method. It has various advantages such as computational efficiency, numerical stability, reduced programming effort and reduced computational time. Planar waveguides having longitudinal discontinuities can be analyzed using this method as it can account for the backward reflected field. Analysis of single discontinuity [18, 19] and multiple discontinuities [20-24] in optical waveguides, using the MOL, have been reported in the literature. It has also been applied to solve non-linear waveguide problems [25] as well as diffraction problem from waveguide ends [26].

2.2 Basic Algorithm

The analysis to be done in this thesis work is limited to the two-dimensional space (x-z). For the waveguide structure under investigation, the waveguide geometry is discretized in the transverse direction (x-axis) and then solved analytically in the direction of wave propagation (z-axis). Figure 2.1 shows a planar waveguide in which the interfaces of layers are parallel to the z-axis. The computational window in the transverse direction is bounded by an electric wall where $E_y = 0$ or a magnetic wall where $H_y = 0$ as appropriate and Δx represents the mesh size. The coordinate system used throughout this thesis is also shown in the same figure. Initially, the mesh size Δx is kept uniform by placing the discretization points equidistant. But, there are some instances where non-uniform mesh size might be more advantageous and will be discussed later.

Consider the two dimensional wave equation:

$$\frac{\partial^2 \psi(x,z)}{\partial z^2} + \frac{\partial^2 \psi(x,z)}{\partial x^2} + k_0^2 n^2(x)\psi(x,z) = 0 \qquad (2.1)$$

Where, $\psi = E_y$ (for TE waves) or H_y (for TM waves)

$k_0 = \dfrac{2\pi}{\lambda_0}$ is the free space wave number

λ_0 = Free space wavelength and $n(x)$ = Refractive index of the medium
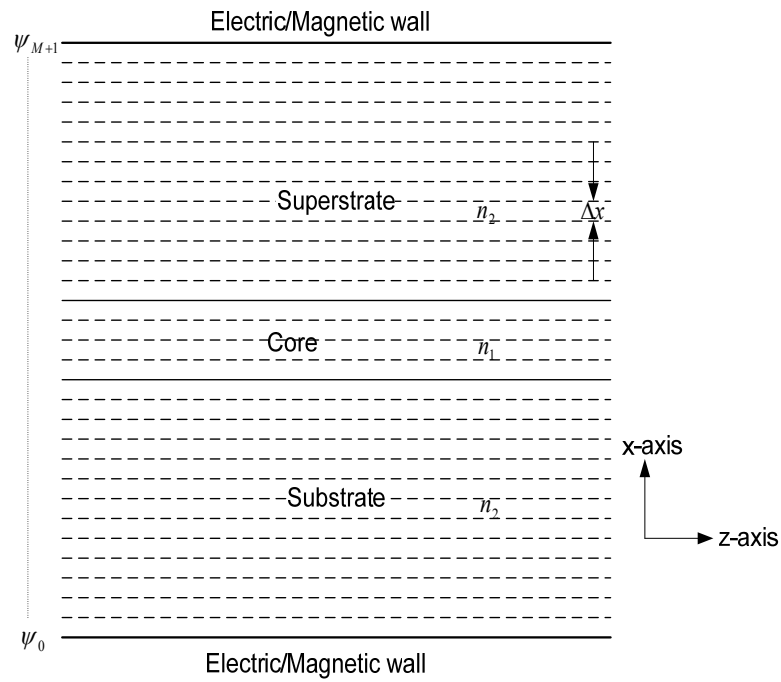
Figure 2.1: Mesh Discretization used in the MOL

Here both the field $\psi(x,z)$ and the refractive index $n(x)$ are discretized along the transverse direction. The $\dfrac{\partial^2}{\partial x^2}$ term in equation (2.1) is replaced by the well-known three-point central difference approximation [10] of the form:

$$\frac{\partial^2 \psi_i}{\partial x^2} = \frac{\psi_{i+1} - 2\psi_i + \psi_{i-1}}{(\Delta x)^2} \qquad (2.2)$$

So that at the *ith* grid point we have:

$$\frac{\partial^2 \psi_i(z)}{\partial z^2} + \frac{\psi_{i+1}(z) - 2\psi_i(z) + \psi_{i-1}(z)}{(\Delta x)^2} + k_0^2 n_i^2 \psi_i(z) = 0 \qquad (2.3)$$

When equation (2.3) is applied at each of the M discrete lines, we get M distinct equations, which can be assembled together in a single matrix equation of the form:

$$\frac{d^2}{dz^2} \begin{bmatrix} \psi_1(z) \\ \psi_2(z) \\ \psi_3(z) \\ \vdots \\ \vdots \\ \vdots \\ \psi_M(z) \end{bmatrix} + \frac{1}{(\Delta x)^2} \begin{bmatrix} -2 & 1 & & & & & \\ 1 & -2 & 1 & & & 0 & \\ & 1 & -2 & 1 & & & \\ & & \ddots & \ddots & \ddots & & \\ & & & 1 & -2 & 1 & \\ & 0 & & & 1 & -2 & 1 \\ & & & & & 1 & -2 \end{bmatrix} \begin{bmatrix} \psi_1(z) \\ \psi_2(z) \\ \psi_3(z) \\ \vdots \\ \vdots \\ \vdots \\ \psi_M(z) \end{bmatrix}$$

$$+ \; k_0^2 \begin{bmatrix} n_1^2 & & & & & \\ & n_2^2 & & & & 0 \\ & & n_3^2 & & & \\ & & & n_4^2 & & \\ & & & & \ddots & \\ 0 & & & & & \ddots \\ & & & & & & n_M^2 \end{bmatrix} \begin{bmatrix} \psi_1(z) \\ \psi_2(z) \\ \psi_3(z) \\ \vdots \\ \vdots \\ \vdots \\ \psi_3(z) \end{bmatrix} = \begin{bmatrix} 0 \\ 0 \\ 0 \\ \vdots \\ \vdots \\ \vdots \\ 0 \end{bmatrix} \qquad (2.4)$$

Written in a compact notation, we get:

$$\frac{d^2}{dz^2}\psi + \frac{1}{(\Delta x)^2}C\psi + k_0^2 N\psi = 0 \qquad (2.5)$$

where, C is a tri-diagonal second-order central-difference matrix, N is a diagonal matrix whose elements are $n_1^2, n_2^2, \ldots, n_M^2$ and $\psi = [\psi_1(z), \psi_2(z), \ldots, \psi_M(z)]^t$ represents the discretized field. The above equation may be written in the form:

$$\frac{d^2}{dz^2}\psi + Q\psi = 0 \qquad (2.6)$$

where,

$$Q = \frac{1}{(\Delta x)^2}C + k_0^2 N \qquad (2.7)$$

The solution of this 2nd-order ordinary matrix differential equation is formally given by [27]:

$$\psi = e^{j\sqrt{Q}z}A + e^{-j\sqrt{Q}z}B \qquad (2.8)$$

where, $e^{j\sqrt{Q}z}$ represents field propagation in the $+z$ direction and $e^{-j\sqrt{Q}z}$ represents field propagation in $-z$ direction. The matrices $e^{j\sqrt{Q}z}$ and $e^{-j\sqrt{Q}z}$ are calculated by diagonalizing the matrix Q to find the eigenvalues and eigenvectors. Q maybe written in the form:

$$Q = UVU^{-1} \tag{2.9}$$

where, U is eigenvector matrix and V is a diagonal matrix containing the eigenvalues of Q. The matrix exponent is then calculated using the following relation:

$$e^{\pm j\sqrt{Q}z} = Ue^{\pm j\sqrt{V}z}U^{-1} \tag{2.10}$$

2.3 Interface conditions

Almost all waveguides used in integrated optics are multi-layered and asymmetric in nature (i.e. the refractive indices of all the layers are different). Thus, the material properties remain uniform within each layer and change abruptly from one layer to the next at the interface. In order to correctly model the electric and magnetic fields at these interfaces, the interface conditions should be appropriately included in the MOL formulation. Using Maxwell equations, it can be shown that [28]:

$$E_y^+ = E_y^- \qquad \text{and} \qquad \frac{\partial E_y^{0^+}}{\partial x} = \frac{\partial E_y^{0^-}}{\partial x} \qquad \text{(For TE)} \tag{2.11}$$

and

$$H_y^+ = H_y^- \qquad \text{and} \qquad \frac{1}{n_2^2}\frac{\partial H_y^{0^+}}{\partial x} = \frac{1}{n_1^2}\frac{\partial H_y^{0^-}}{\partial x} \qquad \text{(For TM)} \qquad (2.12)$$

Therefore from the above equations it can be concluded that, for TE polarization the tangential electric field E_y and its first derivative are both continuous and for TM polarization the tangential magnetic field H_y and $\frac{1}{n^2}\frac{\partial H_y}{\partial x}$ are continuous. All the higher order derivatives of both E_y and H_y with respect to x are discontinuous.

2.4 Non-Uniform Mesh Size

For a multi-layer structure, the widths of different layers may exhibit extreme differences which results in increasing the number of mesh points and consequently the associated computational time and memory requirements. For such instances, it might be more advantageous to have non-equidistant discretizations, leading to a non-uniform mesh size. In such cases, the mesh size is increased in regions where the field exhibits slow variations and decreased in regions where the field exhibits fast variations [29, 30].

Using equations (2.11) and (2.12), and the well-known Taylor's series expansion of the field, a general formula to approximate $\frac{\partial^2}{\partial x^2}$ operator for TE and TM polarizations, can be obtained as [28]:

$$\psi_{0^-}'' = \frac{\psi_{+1} - [\tau_{21}\rho_{21} + 1 + 0.5\Delta x_2^2 k_0^2(n_1^2 - n_2^2)]\psi_0 + \tau_{21}\rho_{21}\psi_{-1}}{0.5\Delta x_2(\Delta x_1 \rho_{21} + \Delta x_2)} \qquad (2.13)$$

where,

n_1 and n_2 represents the refractive indices of layers 1 and 2 respectively (see figure 2.2).

Δx_1 and Δx_2 represents the dicretization distances of layers 1 and 2 respectively(see figure 2.2).

ψ represents E_y or H_y depending on the polarization

$\rho_{21} = 1$(for TE polarization) or $\frac{n_2^2}{n_1^2}$(for TM polarization)

$\tau_{21} = \frac{\Delta x_2}{\Delta x_1}$

Equation (2.13) represents the discontinuity in second derivative at the interface. So, this is a better three-point central-difference approximation of the $\frac{\partial^2}{\partial x^2}$ operator since it accounts for the interface conditions and allows the use of a non-uniform mesh size.
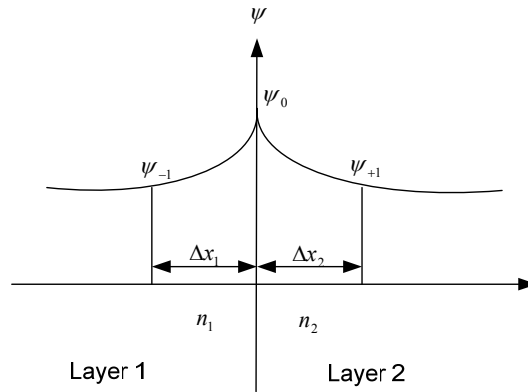
Figure 2.2: Discretized Field in the Transverse Direction.

For a region of uniform refractive index ($n_1 = n_2$) and uniform mesh size ($\Delta x_1 = \Delta x_2$), equation (2.13) reduces to the well-known three-point central-difference approximation, that is:

$$\psi_{0^-}'' \approx \frac{\psi_{+1} - 2\psi_0 + \psi_{-1}}{\Delta x^2} \qquad (2.14)$$

2.5 Absorbing Boundary Conditions

In order to reduce the computational effort, the waveguide is enclosed by a computational window. This computational window is achieved by assuming an electric wall ($E_y = 0$) or magnetic wall ($H_y = 0$) at both edges of the computational window. But, the presence of these walls is undesirable as they cause waves to completely reflect back into the computational

window, leading to erroneous results. Hence, absorbing boundary conditions are necessary in order to improve the accuracy of the calculated results by absorbing the radiated field.

2.5.1 Perfectly Matched Layer (PML)

The PML is an example of an absorbing boundary condition. The PML region is assumed to exist near the boundaries of the computational window and is made sufficiently wide. Then most of the field will be absorbed by the PML and only negligible electromagnetic reflections at the extreme edges of the computational window may occur [31]. The schematic is shown in figure 2.3.

The absorption of the *radiative* wave is done by changing the distance x from *real* to *complex*. This introduces a numerical attenuation factor in the radiative field and hence causes decay of the radiative field in the PML region.

The *real* distance is transformed to a *complex* one according to:

$$x \rightarrow x(1 + j\sigma) \qquad\qquad (2.15)$$

here σ is the decay factor. The wave e^{+jkx} propagating in the $+x$ direction in the real space will be transformed to

$$e^{+jkx(1+j\sigma)} = e^{+jkx}e^{-k\sigma x} \qquad (2.16)$$

in the complex space. The factor $e^{-k\sigma x}$ results in the decay of the field in the $+x$ direction. The choice of the decay factor σ is discussed in [32]. The value of σ may be assumed to be uniform throughout the PML region or else it can be taken as non-uniform [33]. In general

$$(\sigma\Delta x)_i = \left(\frac{\eta}{P}\right)f(x_i) \qquad (2.17)$$

where, $i=1,2,....P$, $(\sigma\Delta x)_i$ represents the value of the imaginary part of the mesh size σ at the ith mesh point in the PML, η is the PML strength parameter and P represents the number of mesh points in the PML layer. The parameter x_i is chosen as

$$x_i = \frac{i\pi}{2(P+1)} \qquad (2.18)$$

and $f(x_i)$ is an arbitrary increasing function of x_i. In our work $f(x_i)$ is chosen to be the tangent function, that is $f(x_i) = \tan(x_i)$, which has a superior performance compared to other functions.
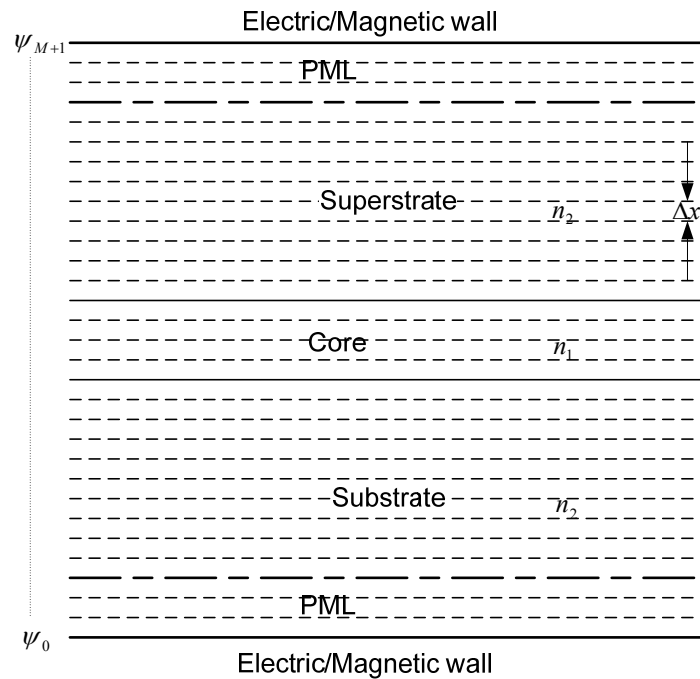
Figure 2.3: PML incorporated with slab waveguide

2.5.2 Numerical Results for PML with Tangent Loss Profile

A numerical routine based on the MOL, which incorporates a non-uniform PML with tangent loss profile has been developed. This routine is used to propagate the Gaussian beam shown in figure 2.4(a) through air (refractive index = 1). The values of P and η are taken as 16 and 1.2 respectively, for both superstrate and substrate. The mesh size is 50nm. The Gaussian beam is propagated for two different cases, with and without the presence of the PML.

It can be seen from the figures 2.4(b) and 2.4(c) that in the absence of PML layer there is interference (represented by the ripples), because the Gaussian beam reflects from the electric

walls back into the computational window as it propagates. However, in the presence of the PML with tangent loss profile there is no interference as there is negligible reflection from the electric walls.
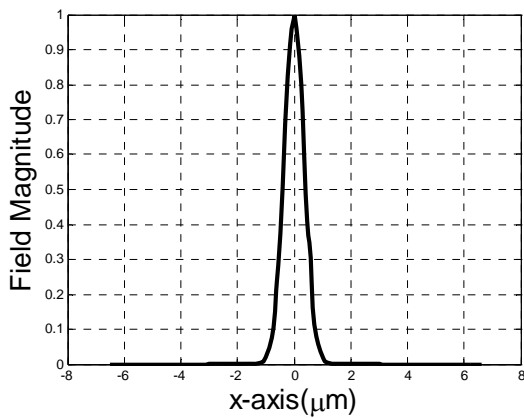
(a) Incident Gaussian Beam at z=0
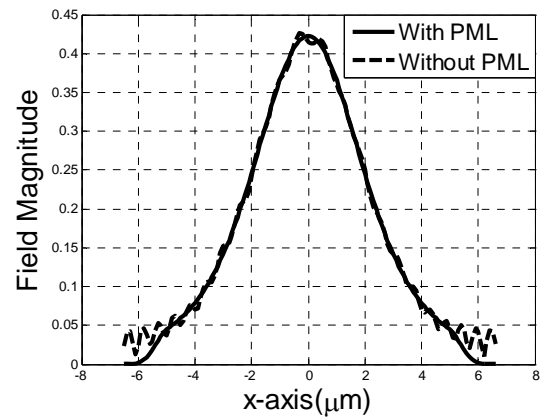
(b) Gaussian Beam at z = 5µm
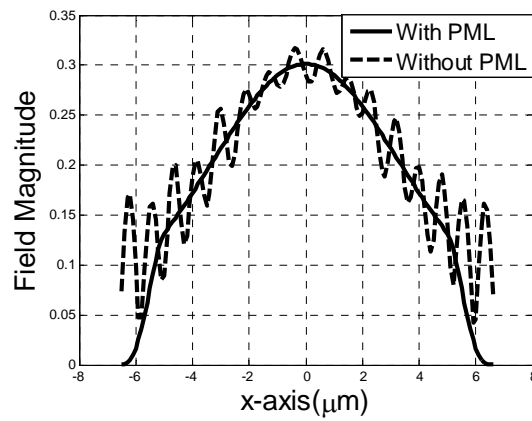
(c) Gaussian beam at z = 10µm

Figure 2.4: Gaussian Beam Propagation with and without the PML.

Chapter 3

MOL Analysis of Longitudinal Waveguide Discontinuities

3.1 Introduction

No device is continuous infinitely. In fact, all practical devices, such as tapers, bends, couplers, mode converters, wavelength filters, etc. display multiple discontinuities. Hence, problems of discontinuity are very important. Discontinuity problems in optical waveguide devices are of considerable theoretical and practical interest. Reflection and transmission occurs at any longitudinal discontinuity and much effort has been made to understand these phenomena. The MOL can account for the transmitted as well as the reflected fields and is very much suitable for the analysis of longitudinal discontinuities in optical waveguides. Analysis of single and multiple waveguide discontinuities using the MOL [34-37] have been reported in the literature. The other methods that have been reported in the literature for the analysis of waveguide discontinuities are the Mode Matching Method [38] and the Equivalent Transmission Network Method [39].

The proposed add/drop filters to be analyzed in this thesis display multiple longitudinal discontinuities. Hence, for their accurate analysis, the MOL must account correctly for the reflection and transmission at these longitudinal discontinuities. In this chapter, we will discuss

analysis of a single waveguide discontinuity and the results obtained from a developed routine will be compared with previously published results in order to signify the accuracy of our implementation.

3.2 Analysis of a Single Waveguide Discontinuity

A frequently faced practical problem is the one where a waveguide sees an abrupt change in the refractive index in the longitudinal direction. This is a situation of a single waveguide discontinuity as shown in figure 3.1. It consists of two regions, region 0 and region 1. The incident field in region 0 results in a backward reflected field in the same region and a transmitted field in region 1. The total field in region 0 is the sum of incident field $e^{+jS_0 z} A_0$ and the reflected field $e^{-jS_0 z} B_0$, and in region 1, only the transmitted field $e^{+jS_1 z} A_1$ exists. A_0, B_0 and A_1 are constant vectors. A_0 and B_0 are the incident and the reflected fields in region 0 at z=0. A_1 is the transmitted field in region 1 at z=0 and $S = \sqrt{Q}$, where Q is defined by equation (2.7) in the previous chapter. The reflected field B_0 and the transmitted field A_1 can be expressed in terms of incident field A_0 as [10]:

$$B_0 = RA_0 \qquad\qquad (3.1)$$

$$A_1 = TA_0 \qquad\qquad (3.2)$$

Where, $R = (I - S_0^{-1}N_0N_1^{-1}S_1)(I + S_0^{-1}N_0N_1^{-1}S_1)^{-1}$ (for TM polarization) or

$$(I - S_0^{-1}S_1)(I + S_0^{-1}S_1)^{-1} \text{ (for TE polarization).}$$

and $T = 2(I + S_0^{-1}N_0N_1^{-1}S_1)^{-1}$ (for TM polarization) or $2(I + S_0^{-1}S_1)^{-1}$ (for TE polarization).
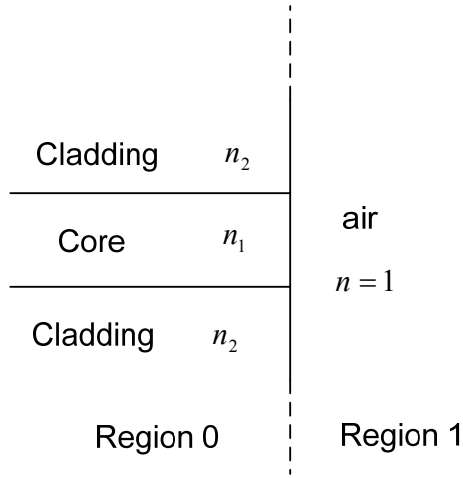
Figure 3.1: A Waveguide Terminated with Air, Leading to a Single Waveguide Discontinuity

3.3 Numerical Results for a Single Discontinuity

A numerical routine based on the MOL with a non-uniform three-point approximation which accounts for interface conditions was developed. In addition, a PML absorber with a non-uniform tangential loss profile has been incorporated into the numerical routine.

The developed routine has been applied to the waveguide structure shown in figure 3.1. The refractive index of the waveguide core, n_1, is considered to be 3.60 and the refractive index of the cladding, n_2, is taken as 3.60(1-Δ). Where, Δ is some parameter. The fundamental TE_0 modal field is assumed to be incident from the left, at a wavelength of 0.86µm. A mesh size of 10nm is used in the analysis. The reflectivity R_0 versus the core width is shown in figure 3.2 for two different values of Δ, one is for Δ=3% (see figure 3.2(a)) and other is for Δ=10% (see figure 3.2 (b)). The core width varies from 0.05 to 1µm. The following matrix relationship has been used to calculate the modal reflectivity:

$$R_0 = \left| \frac{B_0' A_0}{A_o' A_0} \right|^2 \qquad\qquad (3.3)$$

A_0' and B_0' are the transpose of A_0 and B_0, respectively. As seen in figure 3.2, our results compare well with the results of reference [40] signifying the accuracy of our implementation.
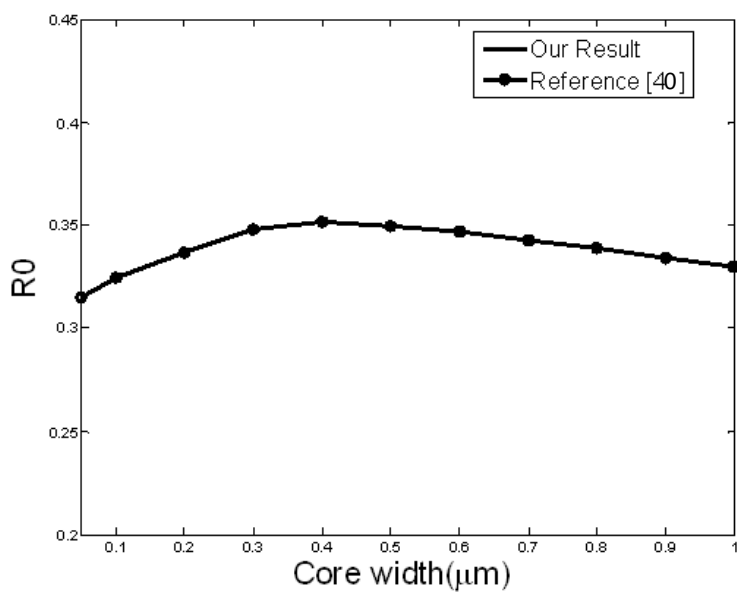
(a) $\Delta=3\%$
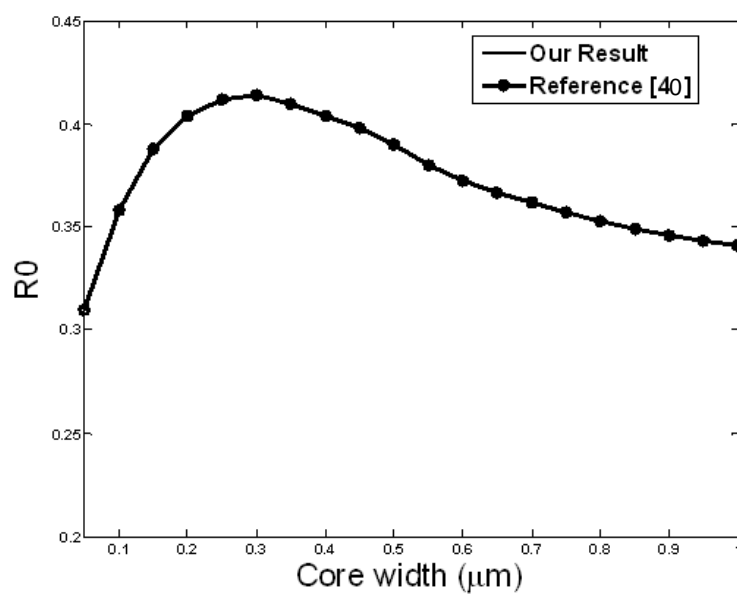
(b) $\Delta=10\%$

Figure 3.2: TE$_0$ Modal Reflectivity R$_0$ versus the Core Width

CHAPTER 4

Directional Coupler and Add/Drop Filter

4.1 Directional coupler

4.1.1 Introduction

A simple yet valuable device is a directional coupler. In its simplest form, it consists of two or more parallel dielectric waveguides in close proximity.

A directional coupler with two parallel waveguides in close proximity is shown in figure 4.1. When an optical signal is launched into one of the waveguides, it is possible to couple the field power to the other waveguide almost completely [41]. The waveguide in which the optical signal is launched is called as the bus and the other waveguide is called the receiver.

$$n_a$$

Input →

Bus n_w Port 2

Port 1

$$n_a$$

Port 4   Receiver n_w Port 3

$$n_a$$
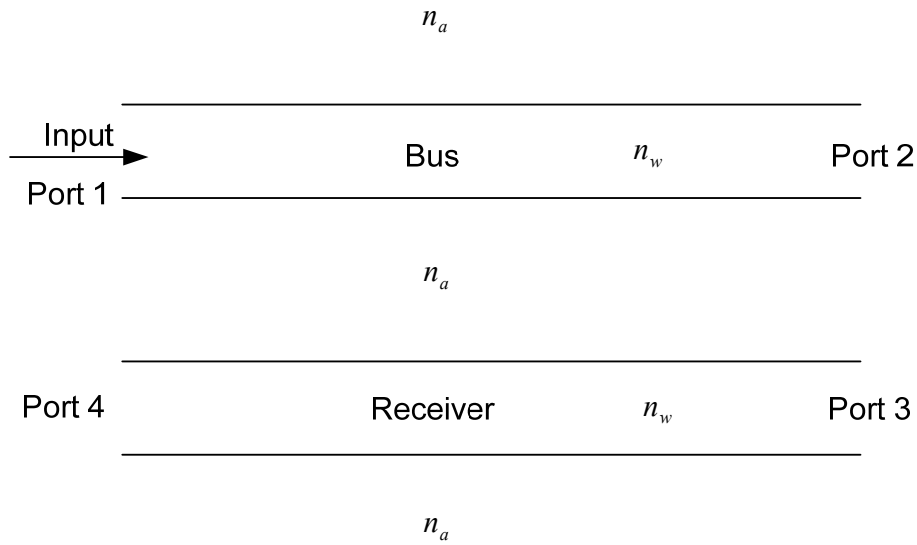
Figure 4.1: Simple directional coupler with two parallel waveguides in close proximity

Depending upon various details of the directional couplers (i.e. separation between them, length of the waveguides, etc.), they can be made to have different properties for different purposes.

4.1.2 Basic Principles

The two waveguides of figure 4.1 are chosen to be single mode and identical. If the waveguides are multimode or not identical, power coupling from one waveguide to another may become very weak [42]. The coupled waveguide structure shown in figure 4.1 supports two modes, an even mode and an odd mode. The signal in both waveguides is in phase for the even mode and 180^0 out of phase for the odd mode. Moreover, the effective refractive index n_{eff} of the even mode is

slightly larger than the effective refractive index n_{eff} of the odd mode. The incident field is obtained by super positioning the even and odd modes. The incident field used in the excitation of the structure is shown in figure 4.2. This input field profile is used throughout this thesis.

The length over which complete power is transferred from the bus waveguide to the receiver waveguide is known as the coupling length (denoted by L_c). It is calculated as:

$$L_C = \frac{\pi}{\Delta\beta} \qquad\qquad (4.1)$$

where, $\Delta\beta$ is the difference of the propagation constants of the even and the odd modes

(i.e. $\Delta\beta = \beta_{even} - \beta_{odd}$).
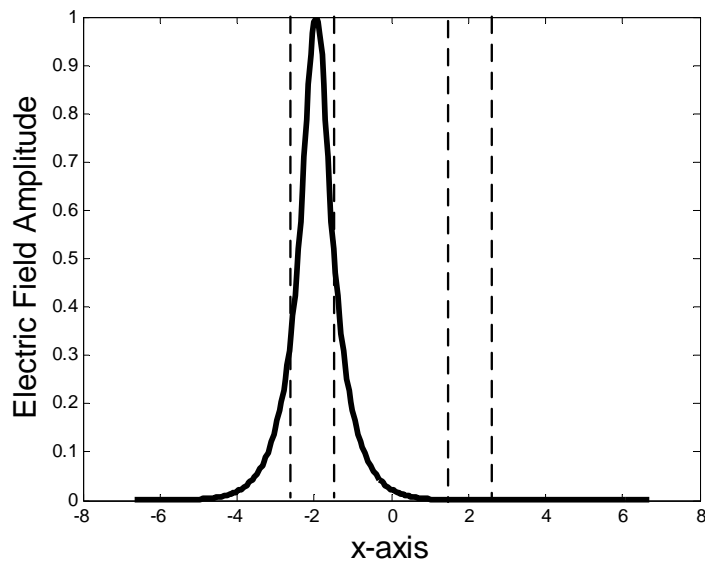
Figure 4.2: Electric Field Amplitude at the Input

4.1.3 Numerical Results for MOL Analysis of Directional Couplers

A numerical routine based on the MOL has been developed to analyze the simple directional coupler shown in figure 4.1. The left side of the bus is referred to as port 1 and the right side is referred to as port 2. The left side of the receiver is referred to as Port 4 and the right side is referred to Port 3. The TE_0 mode pattern of an isolated waveguide shown in figure 4.2 is used as input, at a wavelength of 1.55µm. The refractive index of both waveguides is 3.5 and the surrounding media have a refractive index of 3.4. The separation between the waveguides is 3.4µm and the core width of both waveguides is 0.5µm. The mesh size is fixed at 50nm. Figure 4.3 shows the propagation of the TE_0 mode at different points along the directional coupler. From the figure it can be seen that the coupling length is about 14210µm.
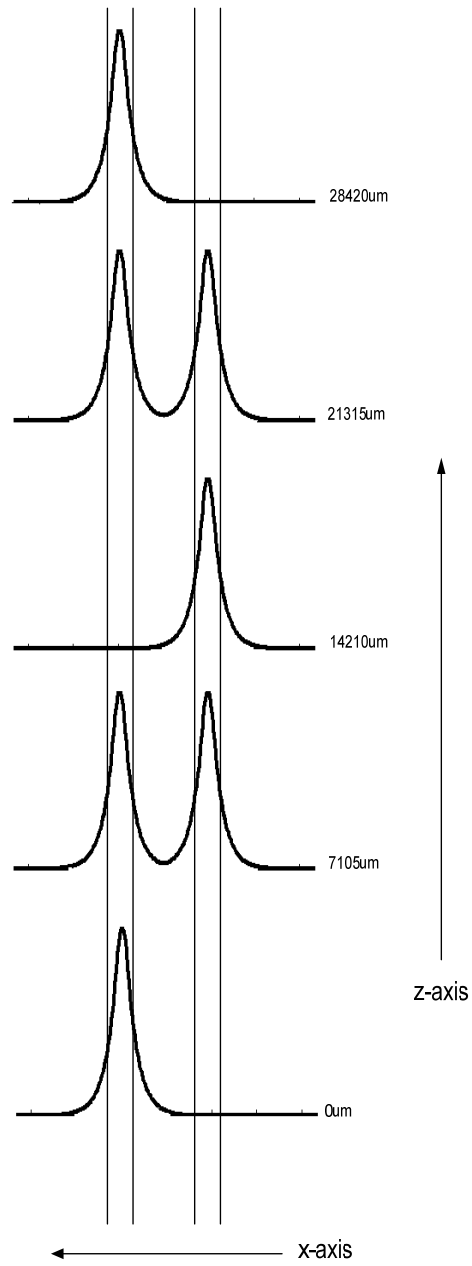
Figure 4.3: Propagation of the TE$_0$ mode at different points along the directional coupler

4.2 Add/Drop Filters

4.2.1 Introduction

When the two waveguides forming the directional coupler (see figure 4.1) are sufficiently isolated from each other, no coupling takes place. A suitable resonant cavity is imbedded between two parallel waveguides resulting in an add/drop filter.

Add/drop wavelength filters with resonant cavities of various shapes have been reported in the literature [10-17]. This includes filters that utilize square, octagonal, hexagonal, circular, ring and elliptically-shaped cavities.

When an optical signal that operates away from resonance is launched into the bus, it will exit through the other side of the bus. However, at resonance, part or all of the optical signal power will be coupled to the receiver and optical power will exit the device through one of the receiver's terminals.

4.2.2 Transmissivity and Reflectivity Calculations of Add/Drop Filter

For our case, the top waveguide is the bus and bottom waveguide is the receiver waveguide. The input signal is propagated through port 1 of the bus waveguide and the modal reflectivity at this

port is referred to as *R1*. The modal transmissivity at port 2 of the bus waveguide is referred to as *T2*, the modal transmissivity at port 3 of the receiver waveguide is referred to as *T3* and the modal transmissivity at port 4 of the receiver waveguide is referred to as *T4*.

The modal reflectivity *R1* and transmissivities *T2, T3* and *T4* can be calculated by using the modal orthogonal relation in matrix form as follows [10]:

$$R1 = \left|\frac{B_0' A_0}{A_o' A_0}\right|^2 \tag{4.2}$$

$$T2 = \left|\frac{A_T' A_0}{A_0' A_0}\right|^2 \tag{4.3}$$

$$T3 = \left|\frac{A_T' A_R}{A_R' A_R}\right|^2 \tag{4.4}$$

$$T4 = \left|\frac{B_0' A_R}{A_R' A_R}\right|^2 \tag{4.5}$$

Where, B_0 is the reflected field in region 0, A_0 is the modal field of the isolated bus waveguide (see figure 4.2). A_0' and B_0' are the transpose of A_0 and B_0 respectively. A_T is the transmitted field at the final layer and A_R is the modal field of the isolated receiver waveguide. The power which radiates from the device is known as Fractional Power Radiated (*FPR*) and is calculated as:

$$FPR = 1 - (R1 + T2 + T3 + T4) \qquad (4.6)$$

Thus, *FPR* represents the power which has not been coupled from the bus to the receiver and this power stays in the bus itself.

Chapter 5

Analysis of Add/Drop Filter with a Square Cavity

5.1 Introduction

An add/drop filter is capable of adding and dropping a certain wavelength from a group of wavelengths. High-index contrast micron-sized cavity resonators have been attracting increasing interest because of their compact size and narrow bandwidth. The circular and ring are the most commonly used cavity shapes. However, there exists a short interaction length between the curved cavity sidewall and the straight waveguides which imposes sub-micrometer air-gap spacing for the evanescent coupling. Square cavity has a long interaction length along the entire flat cavity sidewall and is an alternative to increase the air-gap spacing for the evanescent coupling. Moreover, these cavities are favorable for fabrication because of the flat side walls when compared to curved cavities.

In this chapter we will discuss a general procedure (The Layer by Layer Algorithm) for the treatment of multiple discontinuities. We will also analyze the operation of add/drop filters with single and double square cavities using the MOL. The results obtained from a developed routine

will be compared with previously published results in order to signify the accuracy of our implementation.

5.2 The Layer by Layer Algorithm

The Layer by Layer Algorithm is a general procedure which is used along with the MOL for the analysis of multiple waveguide discontinuities [43]. Another algorithm, along with the MOL, which has been reported in the literature for the analysis of multiple waveguide discontinuities, is the Cascading and Doubling Algorithm [44, 45]. The Layer by Layer Algorithm will be used throughout this thesis work to account for multiple waveguide discontinuities in the longitudinal direction.

For the multi-layer structure shown in figure 5.1, the total field in each region along z-axis is the sum of forward and backwards waves. In this algorithm, a square matrix Γ_k, known as the reflection matrix, is introduced and is given by [10]:

$$
\begin{aligned}
\Gamma_k = & \left[\left(I - U_k^{-1} U_{k+1}\right) + \left(I + U_k^{-1} U_{k+1}\right) D_{k+1} \Gamma_{k+1} D_{k+1}\right] \times \\
& \left[\left(I + U_k^{-1} U_{k+1}\right) + \left(I - U_k^{-1} U_{k+1}\right) D_{k+1} \Gamma_{k+1} D_{k+1}\right]^{-1}
\end{aligned}
\tag{5.1}
$$

where, k=0, 1, 2… N; $D_k = \exp(j S_k d_k)$; and

$U_i = N_i^{-1} S_i$ (For TM polarized waves) or S_i (For TE polarized waves)
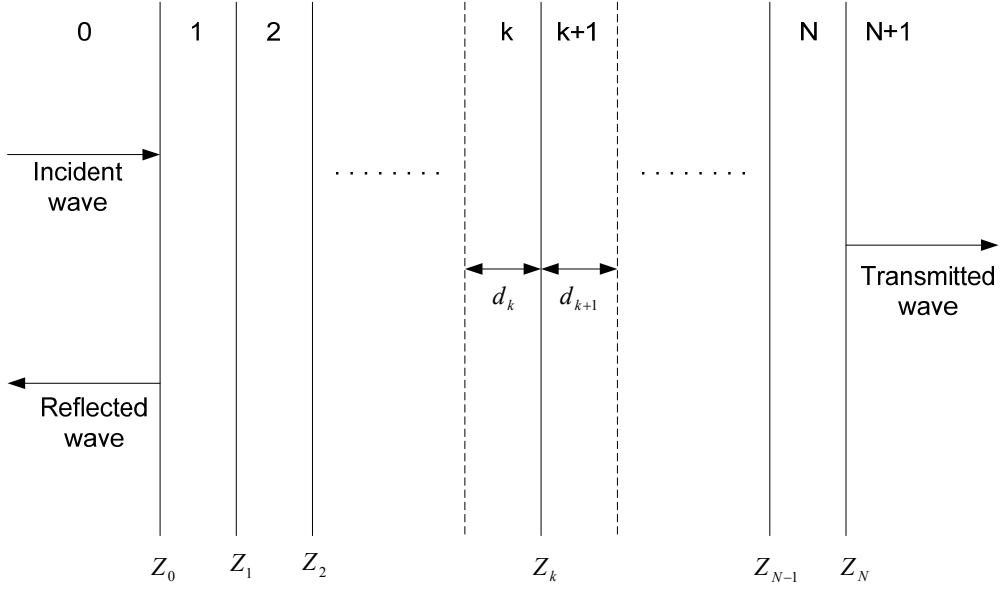
Figure 5.1: Multiple waveguide discontinuities in the z direction

The recursive relation in equation (5.1) expresses the reflection matrix Γ_k of layer k in terms of the reflection matrix Γ_{k+1}. The last layer (transmission layer) has only a forward wave and hence $\Gamma_{N+1} = 0$. We start from the last layer and work backward to find out the reflection matrices until Γ_0 is computed. Using $B_0 = \Gamma_0 D_0 A_0 = \Gamma_0 A_0$ we are able to obtain the reflected field B_0 in terms of the incident field A_0 for any number of discontinuities in z-direction. Then the transmitted field of other regions can be calculated from the following expression:

$$A_{k+1} = 0.5\left[\left(I + U_{k+1}^{-1} U_k\right) D_k A_k + \left(I - U_{k+1}^{-1} U_k\right) B_k\right] \tag{5.2}$$

and the reflected field at any interface can be calculated with the following expression:

$$B_k = \Gamma_k \left(D_k A_k \right) \qquad (5.3)$$

The reader is referred to [10] for more details on the Layer by Layer Algorithm.

5.3 Add/Drop Filter with a Single Square Cavity

A square cavity is placed between two parallel and identical waveguides as shown in figure 5.2. The height and width of the cavity are h and w respectively. For this case h=w. The air-gap between the cavity and the waveguides is g.

The fundamental mode of the isolated waveguide is used as an input at port 1. For a certain dimensions of the cavity and an optimal value of g, a fraction of the optical power is dropped to Port 3 and Port 4 of the receiver at a certain wavelength (i.e. resonant wavelength). A fraction of power is also reflected back to Port 1 of the bus.
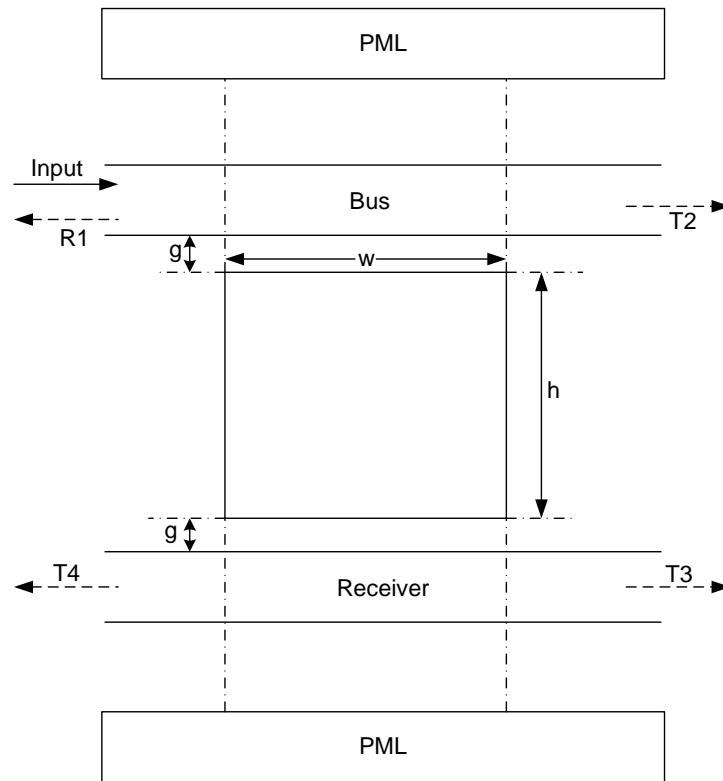
Figure 5.2: Add/Drop Filter with an imbedded Square Cavity between Two Parallel Waveguides

5.3.1 Numerical Results for Add/Drop Filter with Single Square Cavity

The developed numerical routine based on the MOL has been used to analyze add/drop filter with a square imbedded cavity. The waveguides and the cavity have a refractive index of 3.2. The surrounding media is air with a refractive index of 1. The core width of both waveguides is 0.2μm. The modal reflectivity and modal transmissivities of all the ports have been calculated. The mesh size along x-axis is taken as 5.6nm. This small mesh size is required in order to

achieve accurate results. The air gap width g is taken as 0.28μm and the dimensions of the square are 1.54μm.

The waveguide and cavity dimensions are identical to those reported in reference [10]. The calculated results are compared with the results of reference [10] (see figure 5.3). Our results show good agreement with the results of reference [10] signifying the accuracy of our simulations.

The response of the four ports *R1, T2, T3, T4* and *FPR* over the wavelength range of 1.524μm to 1.54μm are shown in figure 5.2. The results show a clear wavelength selectivity of the filter at the resonance wavelength $\lambda \approx 1.532$μm. It can be observed that at the resonant wavelength part of the power is dropped from the upper waveguide into the lower waveguide. The transmissivity at bus port2, *T2*, drops from unity to 0.369 at the resonant wavelength. The reflectivity at bus port1, *R1*, increases from zero to 0.164 and the transmissivity at the receiver ports 3 and 4, *T3* and *T4*, increase to 0.165 and 0.168 respectively at resonance. The fractional power radiated, *FPR,* reaches a maximum value of 0.133 at resonance.
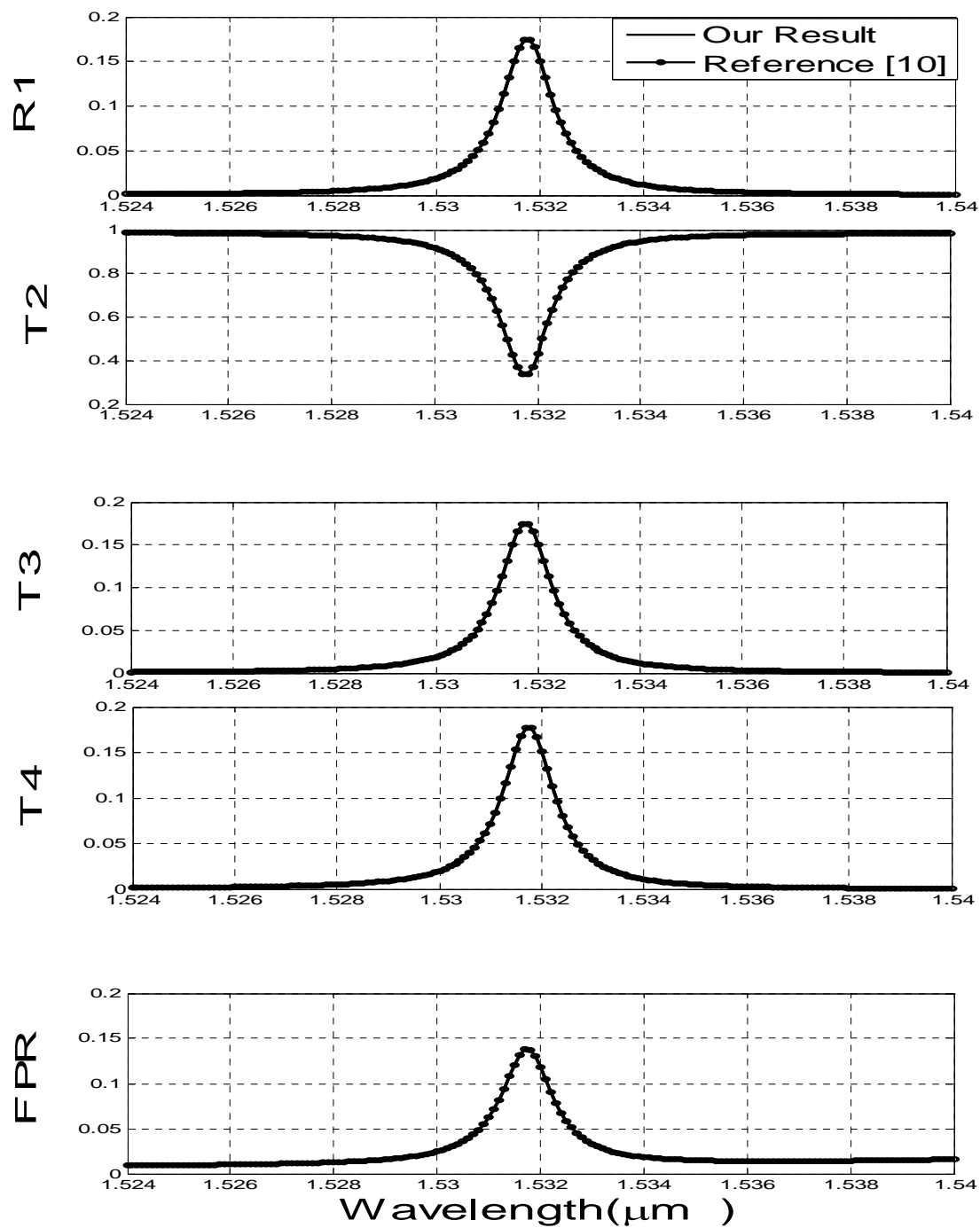
Figure 5.3: Response of the Add/Drop Filter with a Single Square Cavity

5.4 Add/Drop Filter with Two Square Cavities

In order to test the developed routine for multiple discontinuities along the z-axis and to achieve better filtering efficiency, an add/drop filter with two symmetrical square cavities have been analyzed. A schematic is shown in figure 5.4.

The two square cavities are placed in the horizontal direction (see figure 5.4) leading to multiple discontinuities along the z-axis. The air gap between the waveguides and the cavities is g and the separation between the cavities is s.

5.4.1 Numerical Results for Add/Drop Filter with Two Square Cavities

The two identical square cavities are separated by s=0.715µm. All the other parameters are same as the single square case. The results show better response than those with a single square cavity.

As seen in figure 5.5, our results compare well with the results of reference [10] signifying the accuracy of our developed routine.
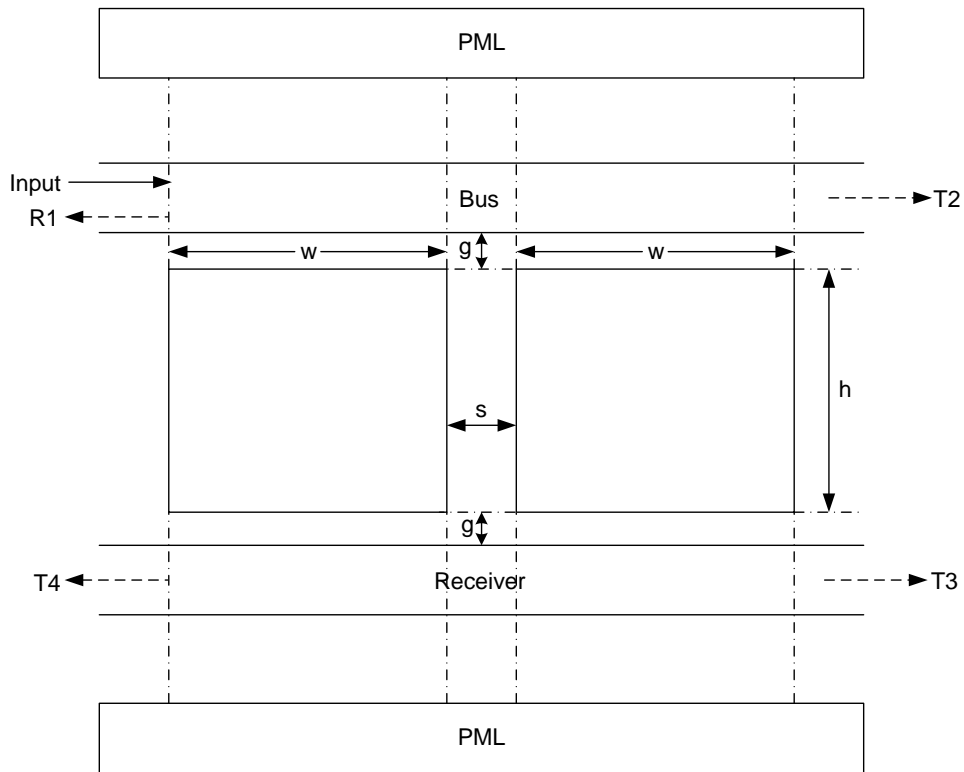
Figure 5.4: Add/Drop Filter with two Square Cavities imbedded between two Parallel
Waveguides.

The response of the four ports *R1, T2, T3, T4* and *FPR* over the wavelength range of 1.52μm to
1.545μm are shown in figure 5.5. From the results it can be seen that the resonant wavelength is
λ = 1.532μm. It can be observed that at the resonant wavelength part of the power is dropped
from the upper waveguide into the lower waveguide. The transmissivity at bus port2, *T2*, drops
from unity to 0.05 at the resonant wavelength. The transmissivity at the receiver ports 3, *T3*,
increases from zero to 0.65 at resonance. *T4* and *R1* are 0.105 at wavelength 1.5315μm and 0.06

at wavelength 1.5325μm. *T4* and *R1* drop down to 0.01 in between 1.5315μm and 1.5325μm. The fractional power radiated, *FPR,* reaches a maximum value of 0.29 at resonance.

Moreover, it can be observed that with two identical cavities, the transmissivity at port3 increases dramatically. This is due to constructive interference between the cavities resonances as mentioned in [46].
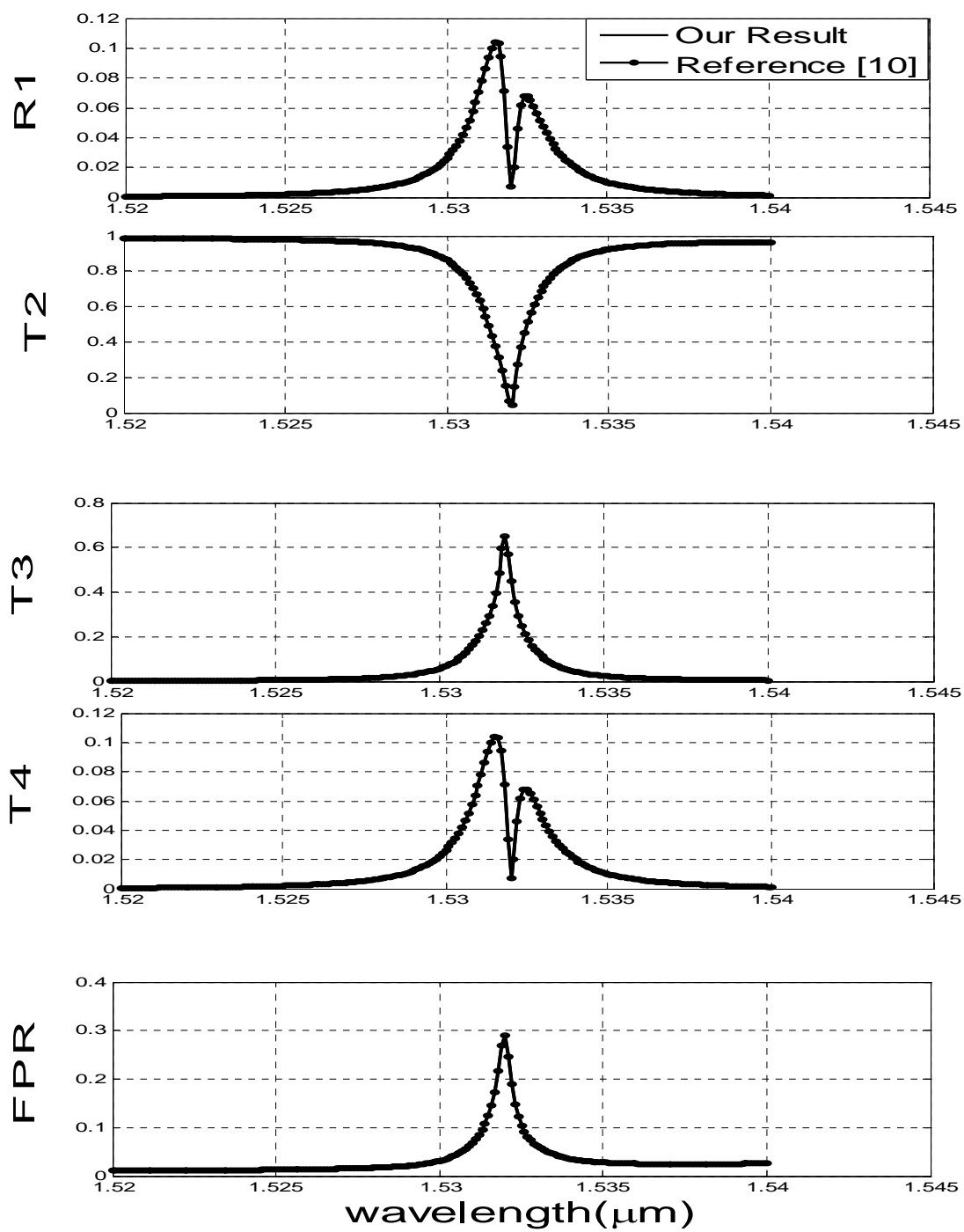
Figure 5.5: Response of Add/Drop Filter with two Square Cavities

Chapter 6

Analysis of Add/Drop Filter with a Rectangular Cavity

6.1 Introduction

In this chapter we analyze the operation of an add/drop filter with a rectangular cavity. We will investigate the effect of this cavity on reflection at port 1 and transmission of the other ports (i.e. port 2, port 3 and port 4). Moreover, the effect of the air gap g and the width w will be investigated.

6.2 Add/Drop Filter with a Rectangular Cavity

Starting with a square cavity, if the height h is fixed and only the width w is varied, then we get a rectangular shaped cavity. Such a cavity is placed between two parallel and identical waveguides as shown in figure 6.1. The air-gap between the cavity and the waveguides is g.

The fundamental mode of the isolated waveguide is used as an input at port 1. At resonance, the input signal will be coupled to the receiver and the power will exit the device through one of the receiver's terminals. A fraction of power is also reflected back to Port 1 of the bus at resonance.
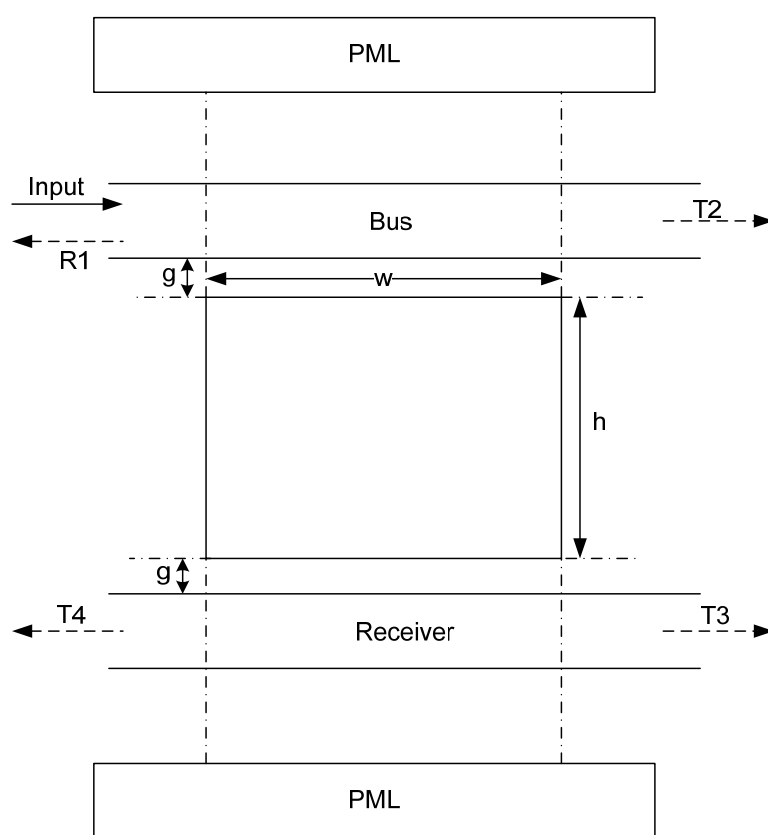
Figure 6.1: Add/Drop Filter with an imbedded Rectangular Cavity between Two Parallel Waveguides

6.2.1 Numerical Results for Add/Drop Filter with a Rectangular Cavity

For the analysis of the above mentioned add/drop filter, a rectangular shaped cavity is imbedded between two parallel and identical waveguides. All the parameters are same as the case for an add/drop filter with a square cavity.

First we analyze the effect of the air gap g by keeping other parameters fixed. Then the effect of the width w is analyzed by fixing other parameters.

Effect of the air gap:

The height h and width w are fixed at 1.54μm and 1.6μm respectively. The spectral response of the four ports (i.e. *R1, T2, T3* and *T4*) for different values of the air gap g is shown in figure 6.2. The air gap varies from 0.21μm to 0.27μm in steps of 0.02μm. From the figure, it can be seen that as the air gap is increased:

I. The resonant wavelength shifts towards higher wavelengths.

II. The spectral width decreases.

III. *T3* and *T4* decrease. This indicates that coupling of power from the bus to the receiver decreases.

IV. Reflection at port 1 and transmission to port 2 also decrease.

V. The peak value remains the same for the fraction of power radiated.

The air gap should neither be too small, because this gives rise to large reflection, nor should it be too large, because this results in very low coupling. Hence, it has to be optimal. We choose g=0.23µm for further analysis. This choice has been made because at this value of g, reflection at the input port is low.
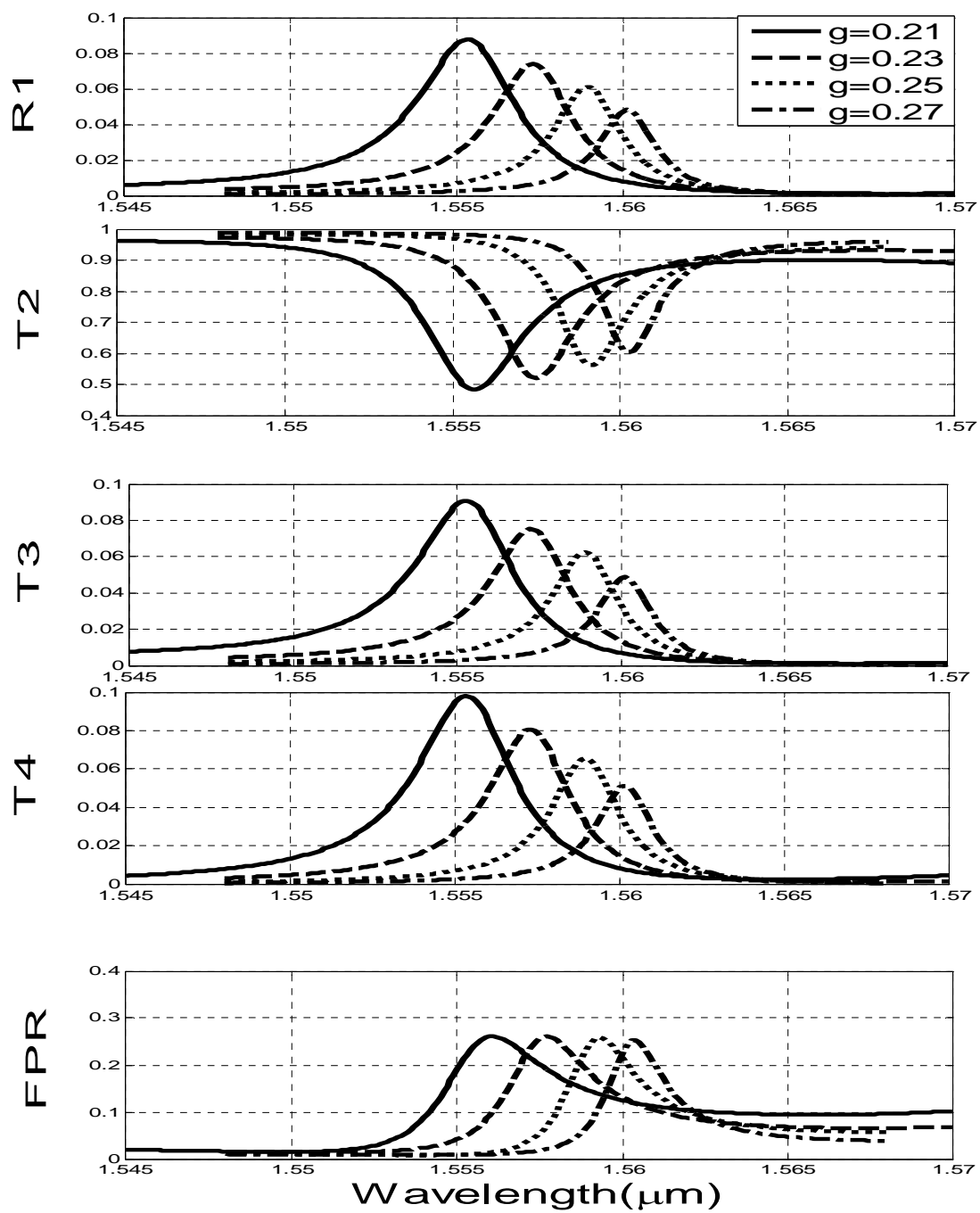
Figure 6.2: Spectral Response of Add/Drop Filter with Rectangular Cavity for different Air Gaps.

Effect of the Width w:

Next, the height h and the air gap g are fixed at 1.54µm and 0.23µm respectively. Figure 6.3 shows the spectral response of the four ports (i.e. *R1, T2, T3* and *T4*) for different values of the width. The width varies from 1.48µm to 1.60µm. From this figure, the following conclusions can be made:

I. The resonant wavelength shifts towards higher wavelengths as the width w increases.

II. The spectral width is minimum for w=1.54µm and increases gradually as w changes.

III. The peaks of *R1, T3* and *T4* reach maximum values for w=1.54µm (i.e. the square case) and they decrease gradually when w is increased or decreased.

IV. Transmission to port 2 is maximum for the square case and decrease gradually as w increases or decreases.

V. The fraction of power radiated is minimum for the square case (i.e. w=1.54µm) and increase gradually with change in w.

Thus, we can see that coupling of power from bus to the receiver is highest for the square case and decreases for the rectangular case. Although reflection is less for the rectangular case when compared to the square case, the power radiation is higher because of low transmission to other ports. Hence, we can conclude that if the volume of a cavity placed between two waveguides increases, the resonant wavelength shifts towards higher wavelengths and if the volume decreases, the resonant wavelength shifts towards lower wavelengths.
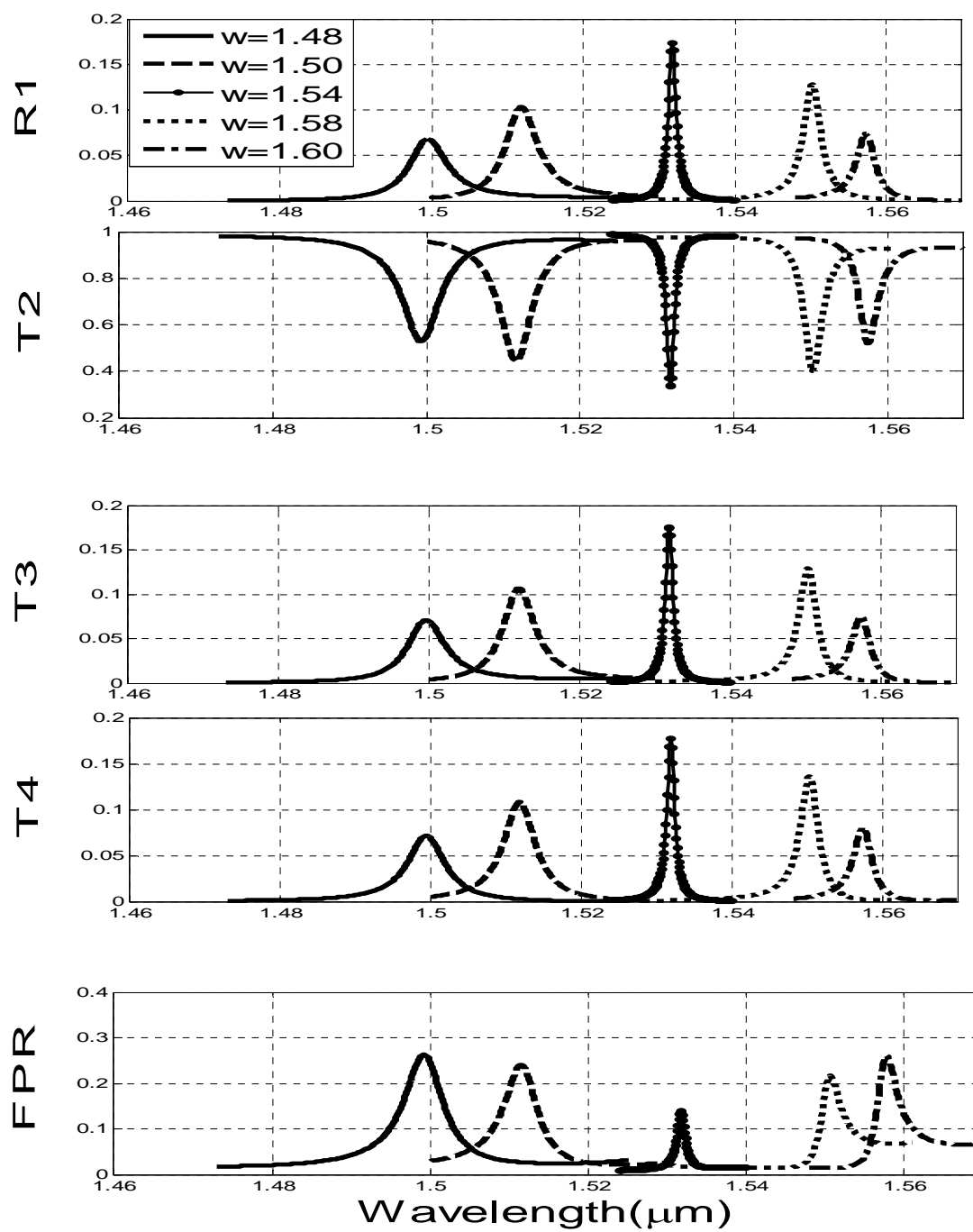
Figure 6.3: Spectral Response of Add/Drop Filter with Rectangular Cavity for different Widths.

Chapter 7

Analysis of Add/Drop Filters with Bow-Tie and Hexagonal Shaped Cavities

7.1 Introduction

For an add/drop filter with square and rectangular cavities as mentioned in chapters 5 and 6 respectively, the evanescent field outside the waveguide sees a sudden discontinuity. Due to this, the reflection at the input port is relatively high. This relatively high reflection is not desirable because it may interfere with the operation of the light source and cause signal distortion, thus reducing the filter efficiency. We expect that if the discontinuity is introduced gradually, the reflection at the input port might decrease. Therefore, we suggest the use of resonant cavities with gradual transition, such as a bow-tie and hexagonal shaped cavities.

In this chapter we analyze the operation of add/drop filters with a bow-tie and a hexagonal shaped cavities. Both the single and double bow-tie shaped cavity cases are considered. A

schematic of a bow-tie shaped cavity placed between two parallel and identical waveguides is shown in figure 7.1. We will investigate the effect of these cavities on the spectral response of all four ports (i.e. port 1, port 2, port 3 and port 4). Moreover, the effect of the air gap g, the width w and the angle θ will also be investigated.
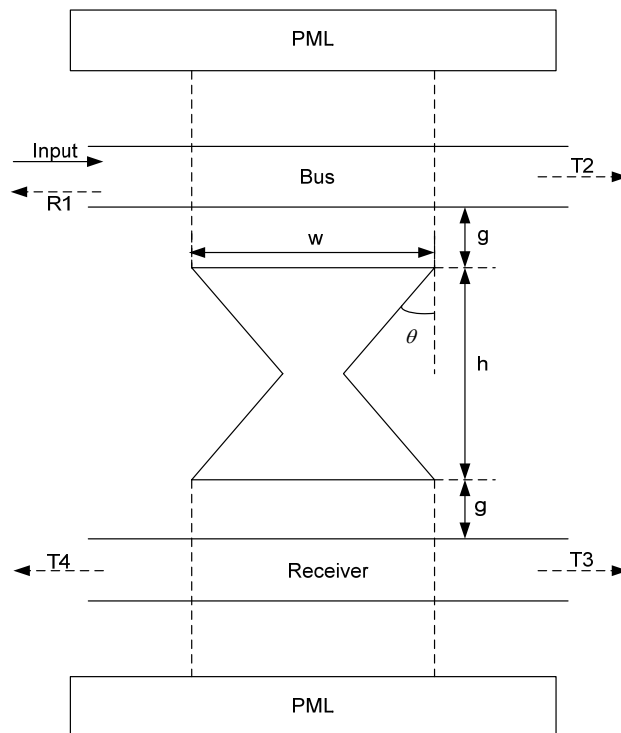
Figure 7.1: Add/Drop Filter with an imbedded Bow-Tie Shaped Cavity between Two Parallel Waveguides

7.2 Add/Drop Filter with a Bow-Tie Shaped Cavity

In a square cavity, if the height h and the width w are fixed and only the center width is decreased, then we get a bow-tie shaped cavity (see figure 7.1). The air gap between the cavity and the waveguides is g and the angle θ represents the amount by which the center width is decreased.

The input (i.e. the fundamental mode of the isolated waveguide) is launched in port 1. At the resonant wavelength, a fraction of the optical power is dropped to Port 3 and Port 4 of the receiver. A fraction of power is also reflected back to Port 1 of the bus at the resonant wavelength.

7.2.1 Numerical Results for Add/Drop Filter with Bow-Tie Shaped Cavity

To analyze this add/drop filter, a bow-tie shaped cavity is imbedded in the developed numerical routine. The waveguides and the cavity have the same refractive index as that used in the previous case. The surrounding medium is air with a refractive index of 1. The Core width of both waveguides and the mesh size along x-axis are also same as the previous case. Initially, the effect of the air gap is analyzed by keeping other parameters fixed. Then, by keeping all

parameters fixed, except θ, the effect of the angle θ is analyzed. Finally, the effect of the width w is analyzed by fixing all other parameters.

Effect of the air gap:

The height h and width w are fixed at 1.54μm and the angle θ is fixed at 2°. The spectral responses of the four ports for different values of the air gap are shown in figure 7.2. The air gap is varied from 0.24μm to 0.28μm in steps of 0.02μm. From the figure, it can be seen that as the air gap is increased:

I. The resonant wavelength shifts towards higher wavelengths.

II. The spectral width decreases.

III. The coupling from bus to the receiver decreases (i.e. *T3* and *T4* both decrease).

IV. Reflection at port 1 and transmission to port 2 also decrease.

V. The fraction of power radiated increases due to decrease in the spectral response of all the ports.

Reflection at port1, *R1*, decreases from 0.187 to 0.136 and transmission to port 3 and port 4 (i.e. *T3* and *T4*) decrease from 0.189 to 0.135 as g is increased from 0.24μm to 0.28μm. Transmission to port 2, *T2*, is 0.33 when g=0.24μm and is 0.41 when g=0.28μm. The fraction of power radiation, *FPR*, increases from 0.125 to 0.21.

Figure 7.2: Spectral Response of Add/Drop Filter with Bow-Tie Shaped Cavity for different Air Gaps.

Effect of the angle θ:

The height h and width w are fixed at 1.54µm and the air-gap g is fixed at 0.28µm. We have chosen the air-gap to be 0.28µm because at this value of g, the reflection at port 1 is relatively low. The spectral responses of four ports (i.e. *R1, T2, T3* and *T4*) for different values of the angle θ are shown in figure 7.3. The angle θ varies from 2° to 5°. From this figure, it can be seen that as the angle θ increases:

I. The resonant wavelength shifts towards shorter wavelengths.

II. Reflection at the input port decreases.

III. Transmission to the other three ports decreases.

IV. The fraction of Power radiated increases to a certain extent.

Thus, we can see that for every 1° change in the angle θ , the shift in the resonant wavelength is approximately equal to 0.011µm. An increase in the angle θ causes the discontinuity to be introduced gradually and as predicted the reflection at the input port, *R1*, decreases. The decrease in *R1* is from 0.14 to 0.04 as θ increases from 2° to 5°. However, minimum transmission at port 2 increases from 0.4 to 0.62 as θ increases from 2° to 5°. The responses of ports 3 and 4 are similar to that of port 1. At resonance the fraction of power radiated increases from 0.2 to 0.216 as θ increases from 2° to 5°.

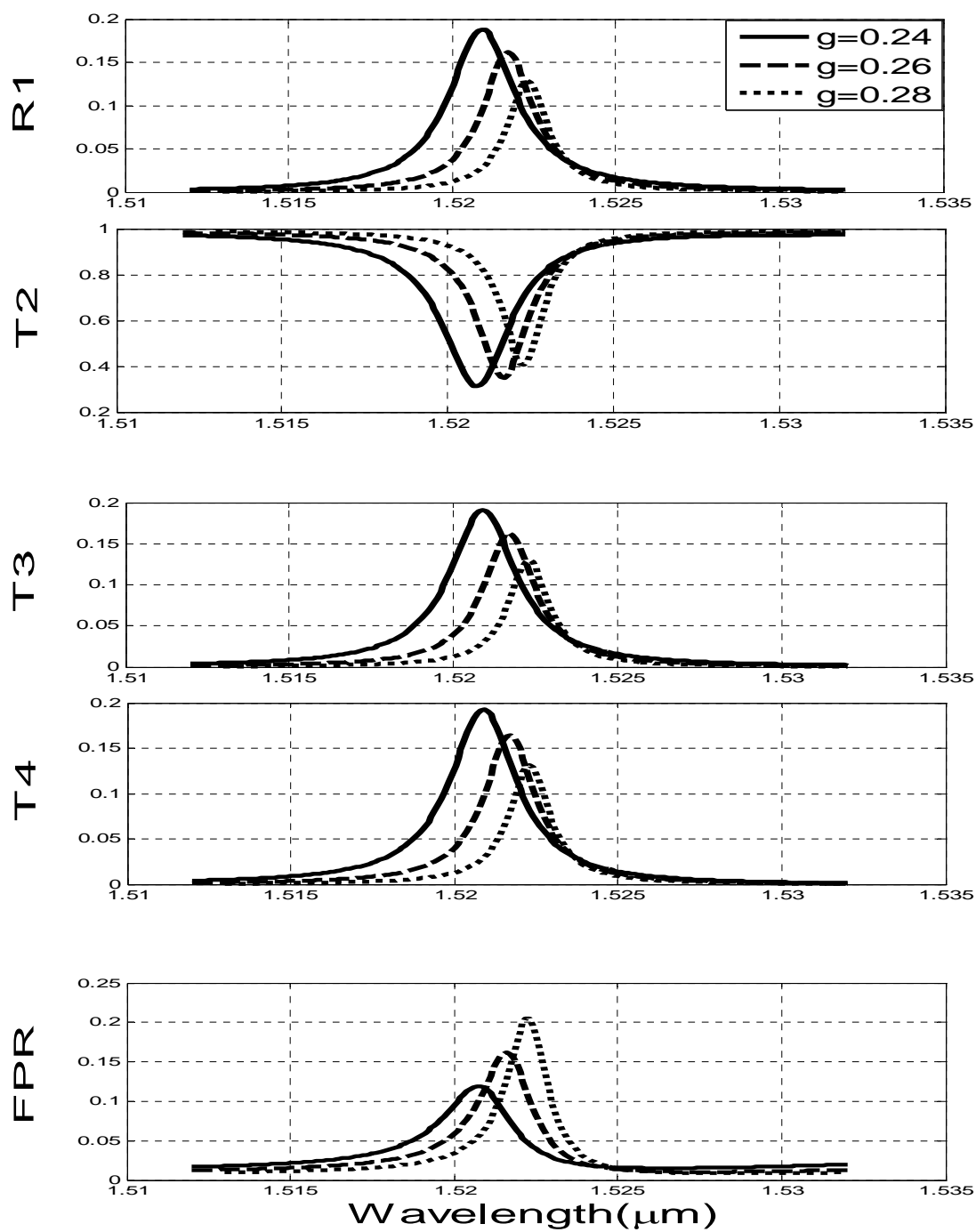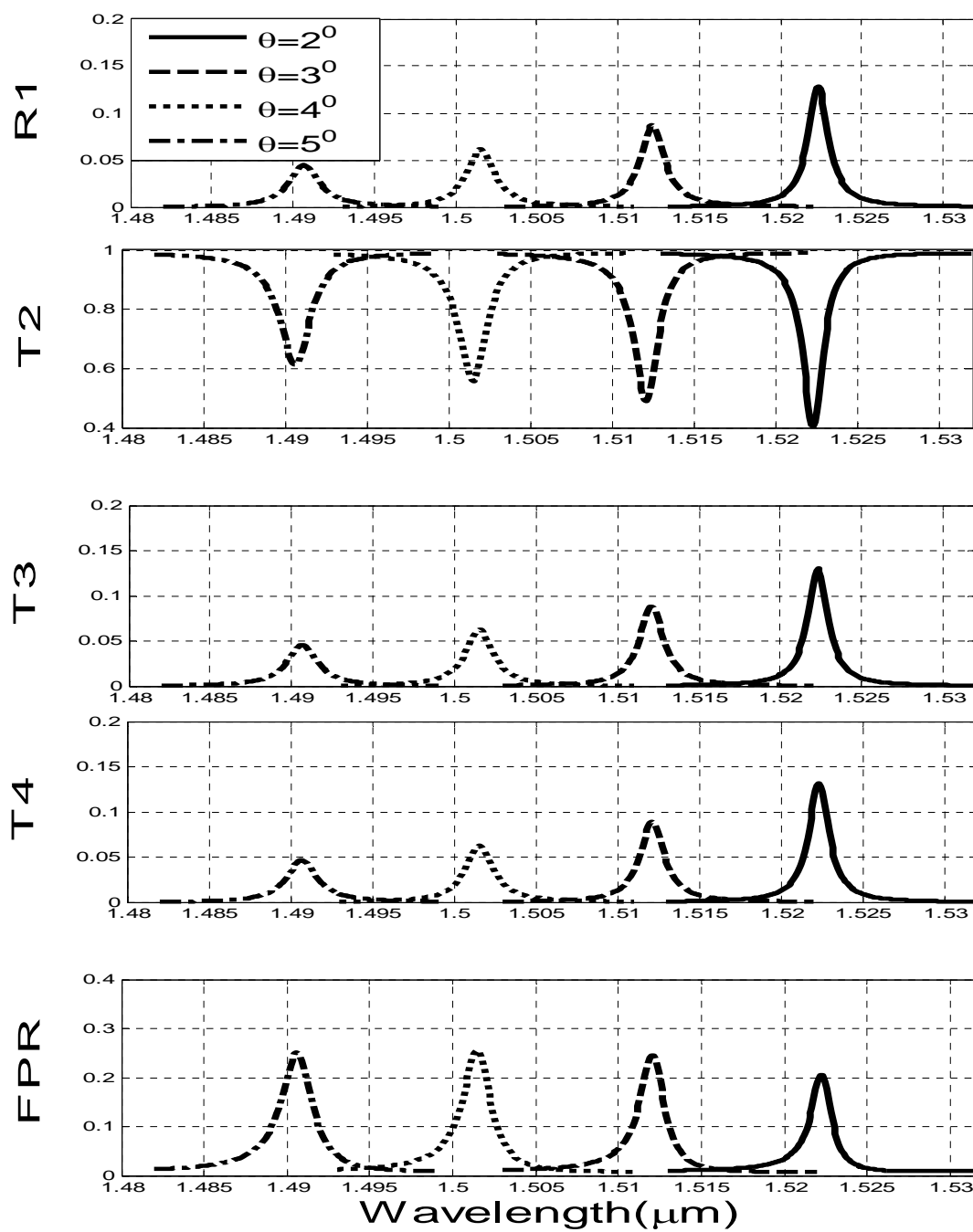Figure 7.3: Spectral Response of Add/Drop Filter with Bow-Tie Shaped Cavity for different Angles.

Effect of the width w:

In order to investigate the effect of the cavity width w, the height h and the air gap width g are fixed at 1.54μm and 0.28μm, respectively. Due to the low reflection at port 1, the angle θ is chosen as 5°. Figure 7.4 shows the spectral response of all the four ports for different values of the width w. The width w is varied from 1.54μm to 1.62μm. It can be seen from the figure that when the width w is increased:

I. The resonant wavelength shifts towards higher wavelengths.

II. The spectral width decreases.

III. Peak reflectivity at the input port and peak transmissivity to all the other three ports increase.

IV. Fraction of power radiated decreases.

An increase in the width w means that the volume of the cavity increases and as discussed in the previous chapter, the resonant wavelength shifts towards longer wavelengths. Peak reflectivity at port 1 increases from 0.041 to 0.119. Peak transmissivity at port 2 improves as its value decreases from 0.62 to 0.42 as w changes from 1.54μm to 1.62μm. Transmission peaks at port 3 and port 4 increase from 0.042 to 0.12 as w is increased from 1.54μm to 1.62μm and this response is almost the same as that of port 1. Fraction of power radiated goes down from 0.25 to 0.21.
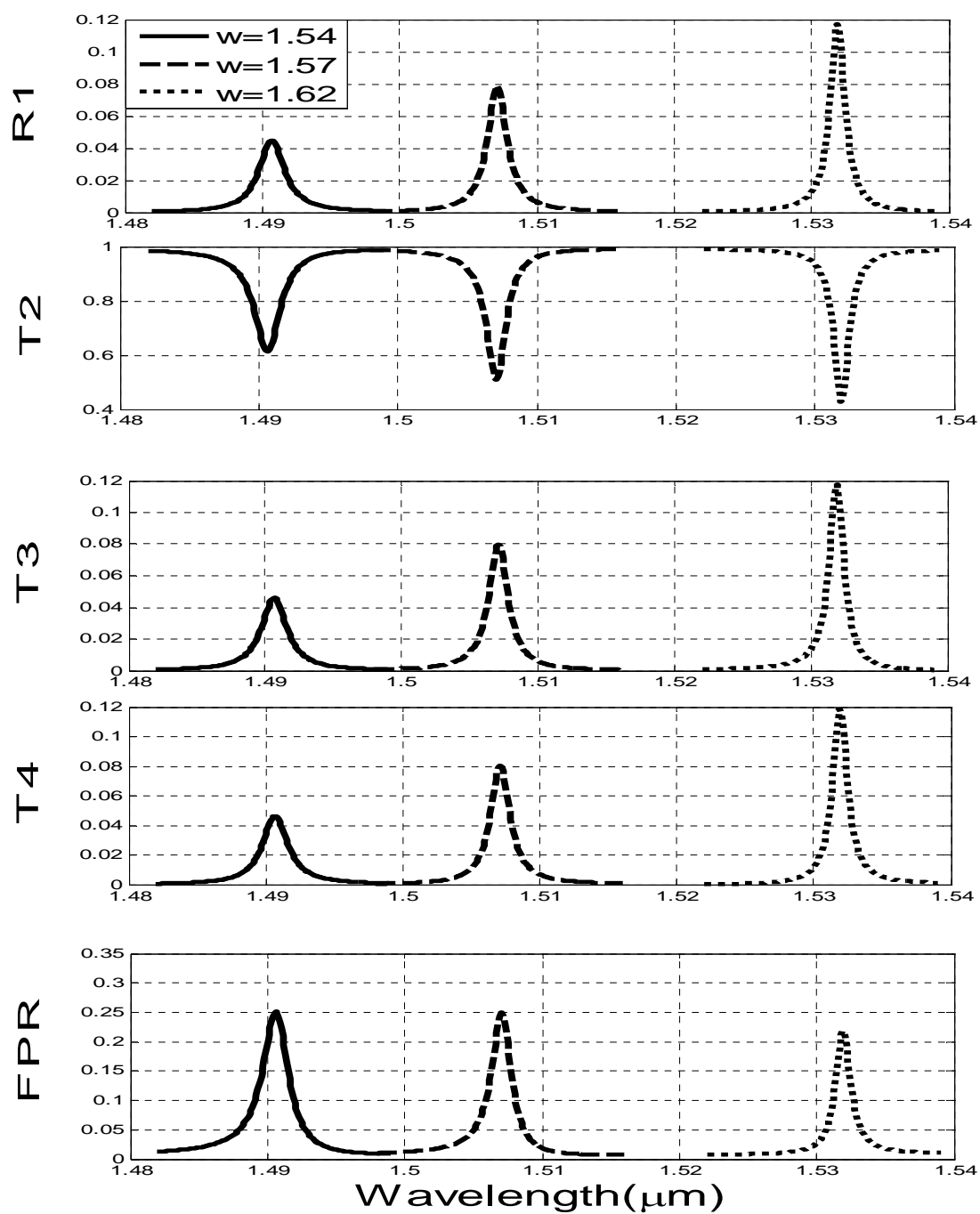
Figure 7.4: Spectral Response of Add/Drop Filter with Bow-Tie Shaped Cavity for different Widths.

7.3 Add/Drop Filter with Two Bow-Tie Shaped Cavities

We have seen that the use of a bow-tie shaped cavity in the add/drop filter, results in reduced reflection at port 1 and also reduced transmission to other ports. In order to improve the filtering efficiency, an add/drop filter with two identical bow-tie shaped cavities, as shown in figure 7.5, has been simulated. All parameters are same as the single bow-tie cavity. The only difference is that there are now two bow-tie shaped cavities instead of one. The separation between the cavities is s.

7.3.1 Numerical Results for Add/Drop Filter with Two Bow-tie Shaped Cavities

An add/drop filter with two bow-tie shaped cavities placed in the horizontal direction (see figure 7.5) has been simulated using the MOL. For both cavities, the height h, the width w, the angle θ and the air-gap g are fixed at 1.54µm, 1.54µm, 2° and 0.28µm respectively. The separation between the cavities s is chosen to be 0.765µm. Figure 7.6 shows a comparison between the spectral responses of the four ports (i.e. *R1, T2, T3* and *T4*) of the add/drop filters with single and double bow-tie shaped cavities. It can be seen that the response of the add/drop filter with two bow-tie shaped cavities is generally better than that with a single bow-tie shaped cavity.
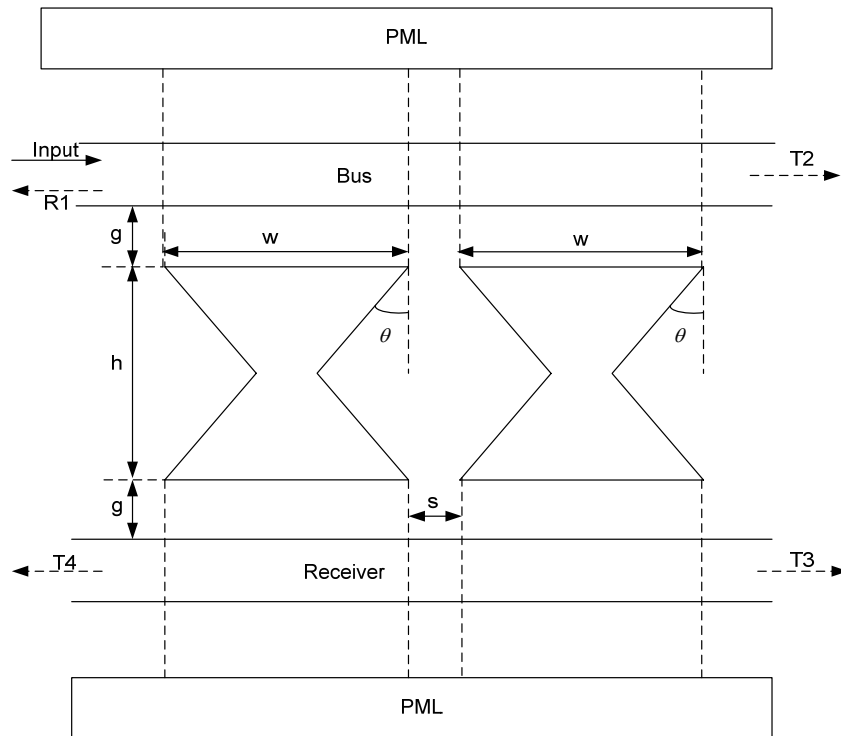
Figure 7.5: Add/Drop Filter with Two Bow-Tie Shaped Cavities imbedded between Two Parallel Waveguides

From the figure it can be seen that the resonant wavelength slightly shifts towards a higher wavelength for an add/drop filter with two bow-tie shaped cavities. The peak reflectivity at port1, *R1*, decreases from 0.187 for a single cavity to 0.035 for two cavities. Minimum modal transmissivity to port 2, *T2*, is reduced from 0.41 to 0.08. The peak transmissivity to port 3, *T3*, increases from 0.135 to 0.58 and the peak transmissivity to port 4, *T4*, decreases from 0.135 to 0.035. However, the maximum fraction of radiated power increases from 0.2 to 0.31. Comparison of spectral responses of an add/drop filter with two bow-tie shaped cavities and an add/drop filter with two square cavities is shown in figure 7.7.
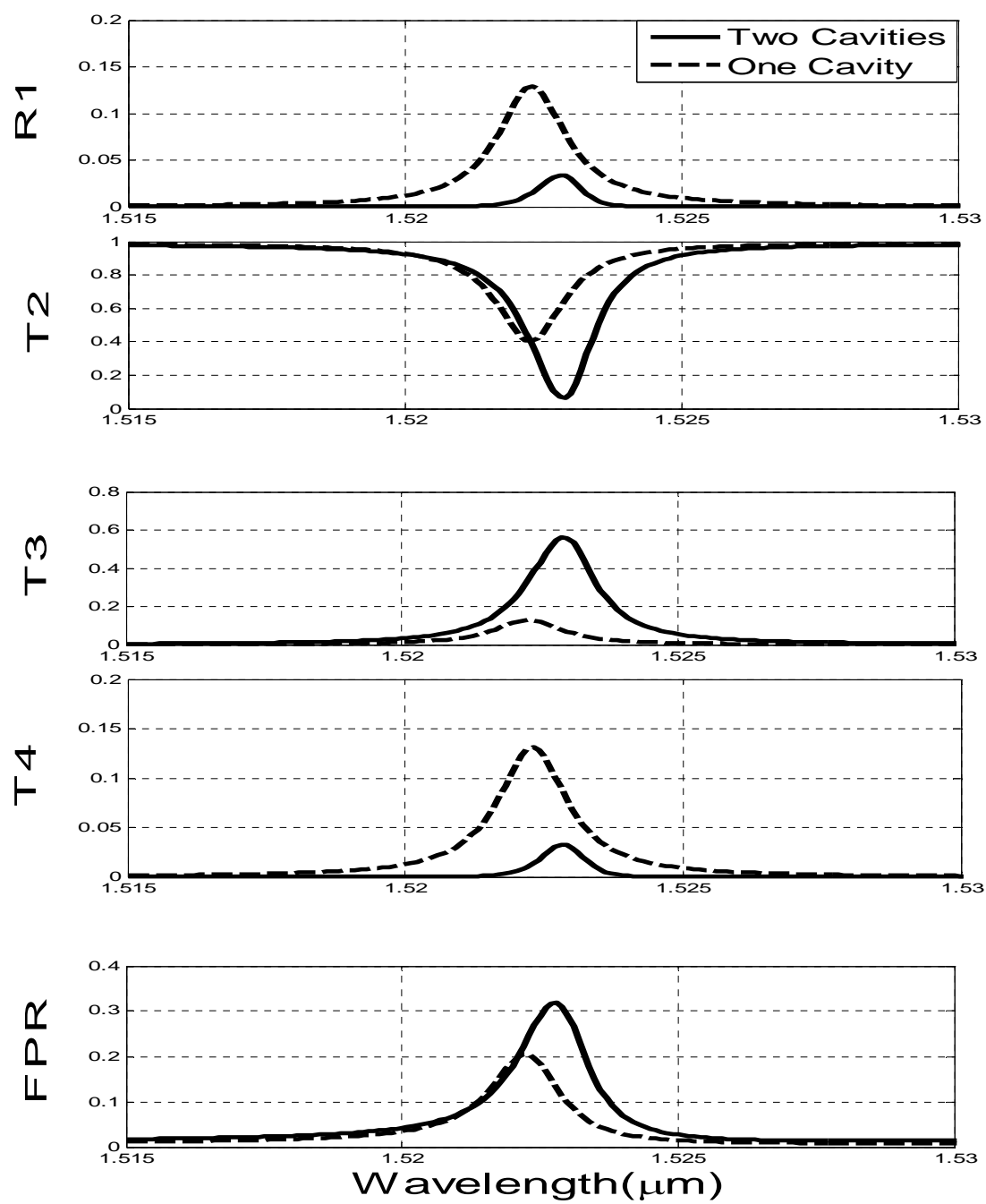
Figure 7.6: Comparison between Add/Drop Filters with Single and Double Bow-Tie Shaped Cavities
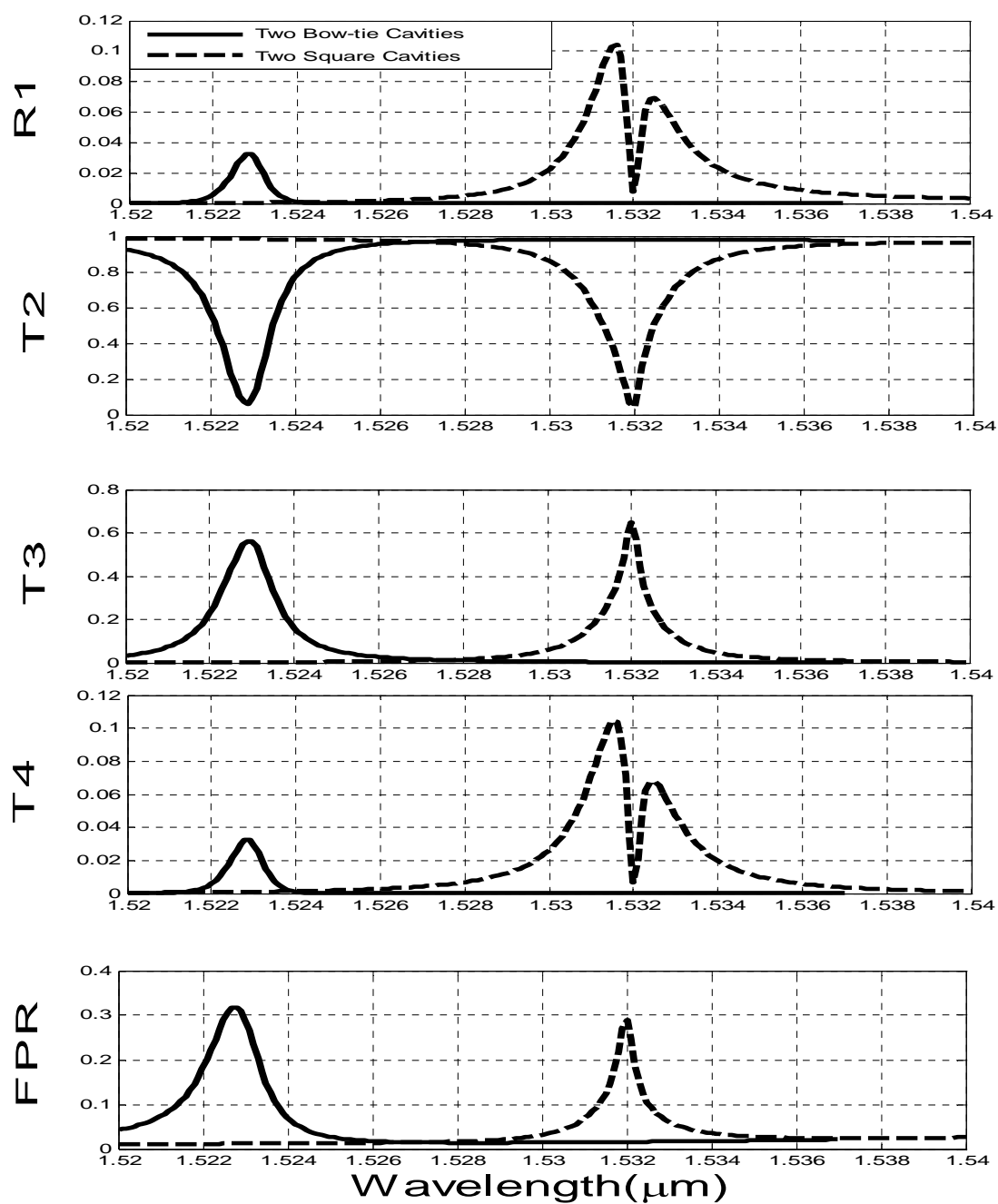
Figure 7.7: Comparison between Add/Drop Filters with Two Bow-Tie and Two Square Cavities

In the two square cavities case, the modal reflectivity, $R1$, exhibits two peaks, while the two bow-tie cavities results in a single peak with a much reduced value. The resonant wavelength in the case of the two bow-tie cavities is different from the two square cavities case. The peak modal reflectivity, $R1$, is reduced from about 0.11 to about 0.035for the double bow-tie cavities case. The modal transmissivity to port 2, $T2$, has a minimum value of 0.08 for the add/drop filter with two bow-tie shaped cavities and it is 0.05 in the two square cavities case. The modal transmissivity to port 3, $T3$, in both cases is high. The peak value of $T3$ equals 0.65 is higher for the add/drop filter with two square cavities compared to 0.58 for the add/drop filter with two bow-tie shaped cavities. The responses of port 4 and port 1 are identical in both cases. The fraction of power radiated has a peak value of 0.305 for the two bow-tie cavities case and 0.29 for the two square cavities case. The responses of port 1 and port 4 are not symmetrical for both cases. Thus, we can clearly see that the use of two bow-tie cavities results in generally improved performance of the add/drop filter when compared to the two square cavities case.

7.4 Add/Drop Filter with a Hexagonal Shaped Cavity

If the height h and the width w of a square cavity are fixed and only the center width is increased, then we get a hexagonal shaped cavity. The schematic of the resulting structure is shown in figure 7.5. The air-gap between the cavity and the waveguides is g and the angle θ corresponds to the amount by which the center width is increased.

The input at port 1 is the same as the previous cases and the spectral responses of all the four ports (i.e. *R1, T2, T3* and *T4*) are obtained.

7.4.1 Numerical Results for Add/Drop Filter with Hexagonal Shaped Cavity

A hexagonal shaped cavity has been incorporated in the developed numerical routine in order to analyze the response of this add/drop filter. The refractive indices, the core width of the waveguides and the mesh size along x-axis are kept same as in the bow-tie shaped cavity case.

As done previously, the effect of the air gap, the angle θ and the cavity width w will be investigated by keeping all other parameters fixed.
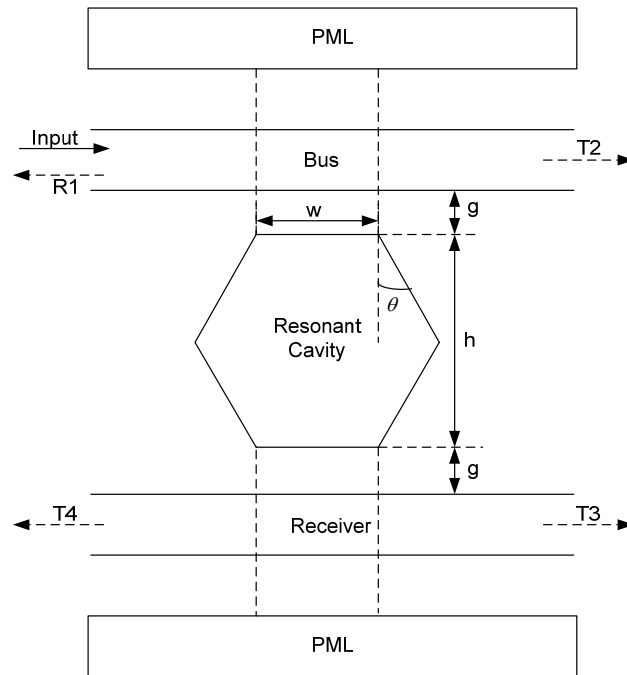
Figure 7.8: Add/Drop Filter with an imbedded Hexagonal Cavity between Two Parallel Waveguides

Effect of the air gap:

The height h, width w and the angle θ are fixed at 1.54μm, 1.54μm and 2° respectively. The spectral response of all the four ports for different values of the air gap widths g, ranging from 0.25μm to 0.32μm is shown in figure 7.9. From this figure, it can be observed that as the air gap is reduced:

I. The resonant wavelength shifts towards lower wavelengths.

II. The spectral width increases.

III. The coupling from the bus to the receiver increases (i.e. both *T3* and *T4* increase).

IV. Reflection at port 1 and transmission to port 2 also increase.

V. The fraction of power radiated decreases because the modal reflectivity at the input port and the modal transmissivity to other three ports increases.

The peak radiated power decreases from 0.17 to 0.13. The modal reflectivity at port 1, *R1*, is 0.15 at g = 0.32μm and has a peak value of 0.185 at g = 0.25μm. The modal transmissivity at port 2 improves as its peak value changes from 0.4 to 0.3. Maximum transmission to port 4 increases from 0.152 to 0.2 and that to port 3 increases from 0.15 to 0.19. We can see that the responses of ports 3, 4 and 1 are almost similar. The value of g is chosen to be 0.28μm for further analysis. When g = 0.28μm, the modal reflectivity at the input port is 0.18. Next, the effect of the angle *θ* will be analyzed.

Figure 7.9: Spectral Response of Add/Drop Filter with Hexagonal Cavity for different Air-Gap Lengths.

Effect of the angle θ :

The height h, width w and the air-gap g are fixed at 1.54μm, 1.54μm and 0.28μm respectively. The spectral response of all the four ports (i.e. *R1, T2, T3* and *T4*) for different values of the angle θ, varying from 2° to 4° is shown in figure 7.10. From this figure, it can be seen that as the angle θ decreases:

I. The resonant wavelength shifts towards lower wavelengths.

II. The spectral width increases.

III. The coupling from the bus to the receiver increases (i.e. both *T3* and *T4* increase).

IV. Reflection at port 1 and transmission to port 2 also increase.

V. The fraction of power radiated decreases.

Increase in the angle θ allows the discontinuity to be introduced gradually and as predicted the reflection at the input port, *R1*, decreases. It can be seen that when the angle θ becomes 4°, the reflection at the input port becomes very low. Moreover, the coupling from bus to the receiver becomes very weak and most of the input power remains in the bus. Responses of port 1, port 3 and port 4 are identical to each other. Fraction of power radiated is highest with a peak value of 0.25 when the angle $\theta=3°$ and lowest with a peak value of 0.12 when the angle $\theta=2°$.
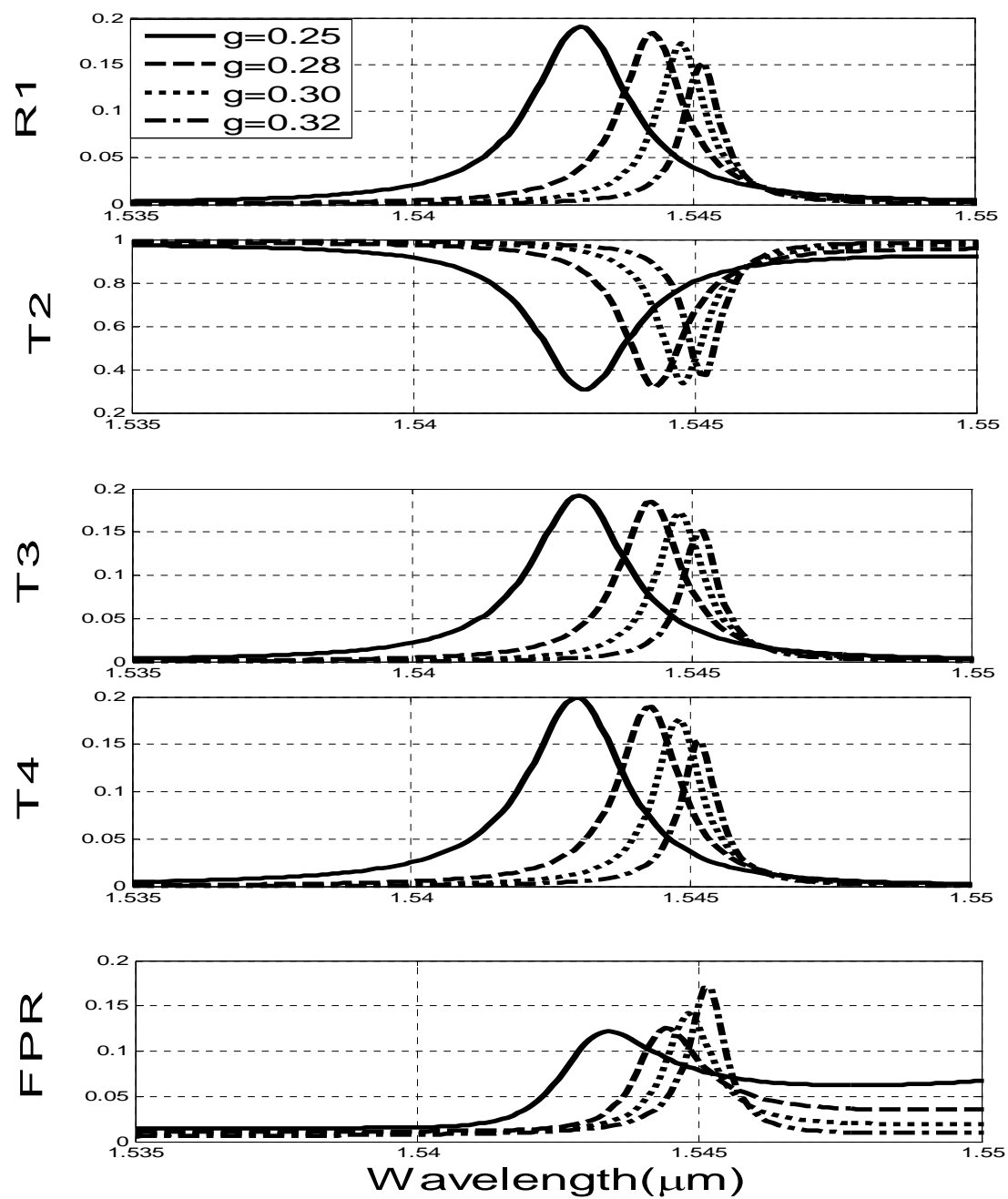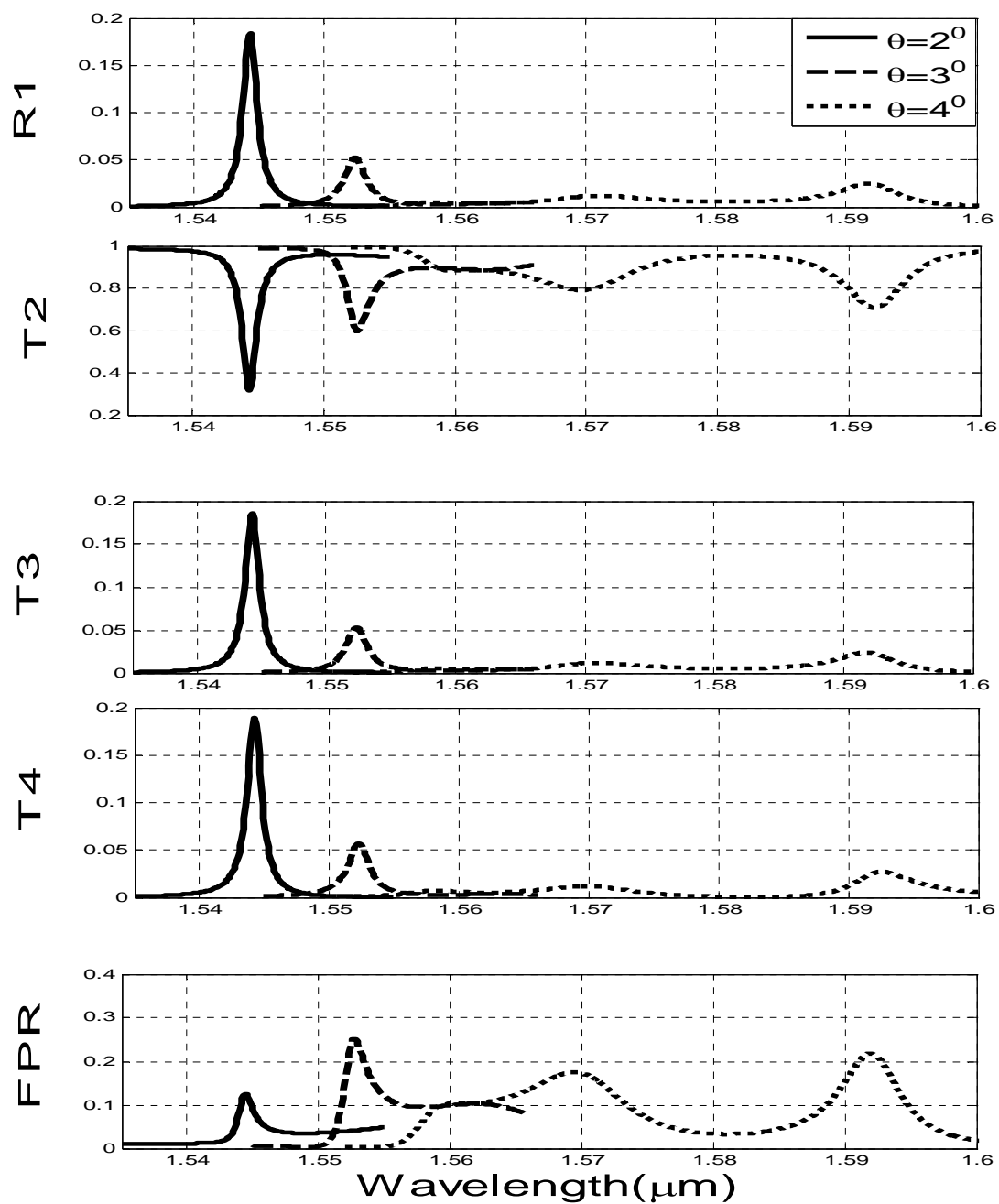
Figure 7.10: Spectral Response of Add/Drop Filter with Hexagonal Cavity for different Air Gaps.

Effect of the width w:

The height h, air-gap g and angle θ are fixed at 1.54μm, 0.28μm and 3° respectively. Figure 7.11 shows the spectral responses of the four ports (i.e. *R1, T2, T3* and *T4*) for different values of width w varying from 1.51μm to 1.57μm. It can be observed from this figure that as the width w decreases:

I. The resonant wavelength shifts towards shorter wavelengths.

II. The coupling from the bus to the receiver increases (i.e. both *T3* and *T4* increase).

III. Reflection at port 1 and transmission to port 2 also increase.

It can be seen from the figure that when the width w = 1.57μm, the dropping performance of the device is very weak and most of the power remains in the bus. At this width, since reflection is also very low, the fraction of radiated power has a peak value of 0.2. The dropping performance improves as the width w increases. The modal reflectivity at port 1, *R1,* is maximum with a peak value of 0.135 at w= 1.51μm and becomes minimum with a peak value of 0.025 at w=1.57μm. The responses of ports 3, 4 and 1 are almost identical. Hence, we can conclude that this device starts to lose its dropping capacity when the angle θ exceeds 3° or the cavity width w becomes less than 1.54μm.
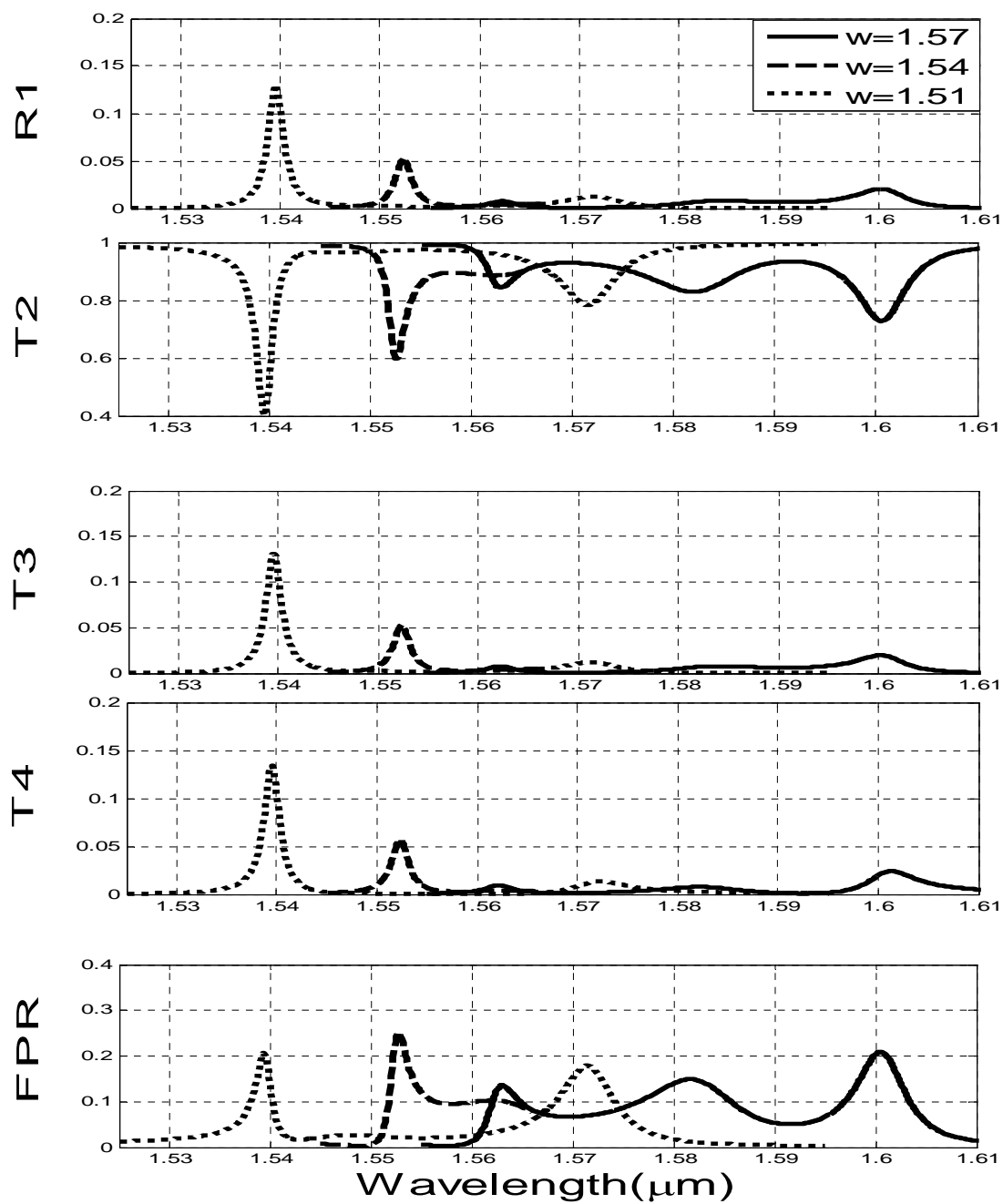
Figure 7.11: Spectral Response of Add/Drop Filter with Hexagonal Cavity for different Widths.

Chapter 8

Analysis of Add/Drop Filter with a

Parallelogram-Shaped Cavity

8.1 Introduction

All the add/drop filters discussed previously have been analyzed by utilizing symmetric cavities. The response of port 3 and port4 are identical to each other when a single symmetric cavity is used. Moreover, the response of port 1 is almost equal to port 3 and port 4. In this chapter, the spectral responses of all the four ports are analyzed for an add/drop filter with an asymmetric cavity. The asymmetric cavity considered is the parallelogram shaped cavity. The effect of the air gap and the width w will be investigated as done previously.

8.2 Add/Drop Filter with a Parallelogram Shaped Cavity Bent towards Left

A parallelogram shaped cavity bent towards left is placed between two parallel and identical waveguides as shown in figure 8.1. This cavity is bent towards left by an angle of 45°. The width, height and the air gap are given by w, h and g, respectively.

8.2.1 Numerical Results for Add/Drop Filter with Parallelogram Shaped Cavity Bent towards Left

A parallelogram shaped cavity, bent towards left, is imbedded in the developed routine and the spectral responses of all the four ports are analyzed. The refractive indices, core widths and the mesh size are the same as considered in the previous cases. First, the effect of air gap g is analyzed in order to find an optimum value of g for this structure. Then, the effect of width w will be analyzed on the response of all the ports.
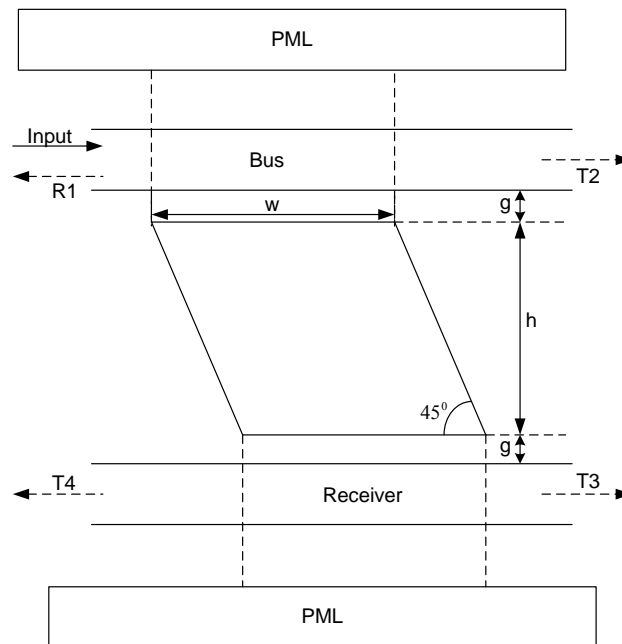
Figure 8.1: Add/Drop Filter with a Parallelogram Shaped Cavity Bent towards Left imbedded

between Two Parallel Waveguides

Effect of the air gap:

The dimensions of the parallelogram are considered the same as that of the square (i.e.1.54µm) and the air gap is varied from 0.25µm to 0.29µm. The effect of varying the air gap g on the spectral response of all the four ports (i.e. *R1, T2, T3* and *T4*) is shown in figure 8.2. From this figure, it can be seen that as the air gap is increased:

I. The resonant wavelength shifts towards higher wavelengths.

II. The spectral width decreases.

III. The coupling from the bus to the receiver decreases (i.e. both *T3* and *T4* decrease).

IV. Reflection at port 1 and transmission to port 2 also decrease.

V. The fraction of power radiated decreases.

The modal reflectivity at port 1 is maximum with a peak value of 0.026 at g=0.25μm and it decreases to 0.013 at g=0.29μm. The modal transmissivity at port 2 increases from 0.65 to 0.75. Peak value of the modal transmissivity at Port 3 decreases from 0.0345 to 0.018. Peak value of the modal transmissivity at Port 4 decreases from 0.025 to 0.012 as g increases from 0.25μm to 0.29μm. The fraction of power radiated decreases from 0.27 to 0.20. Thus, we can see that the responses of Port 3 and Port 4 are not identical. This occurs because of the asymmetric shape of the cavity. Since the parallelogram shaped cavity is bent towards left side (see figure 8.1), the receiver is biased towards port 3 and hence the response of port 3 is better than that of port 4. Moreover, the response of port 1 is no longer identical to either of the ports of the receiver.
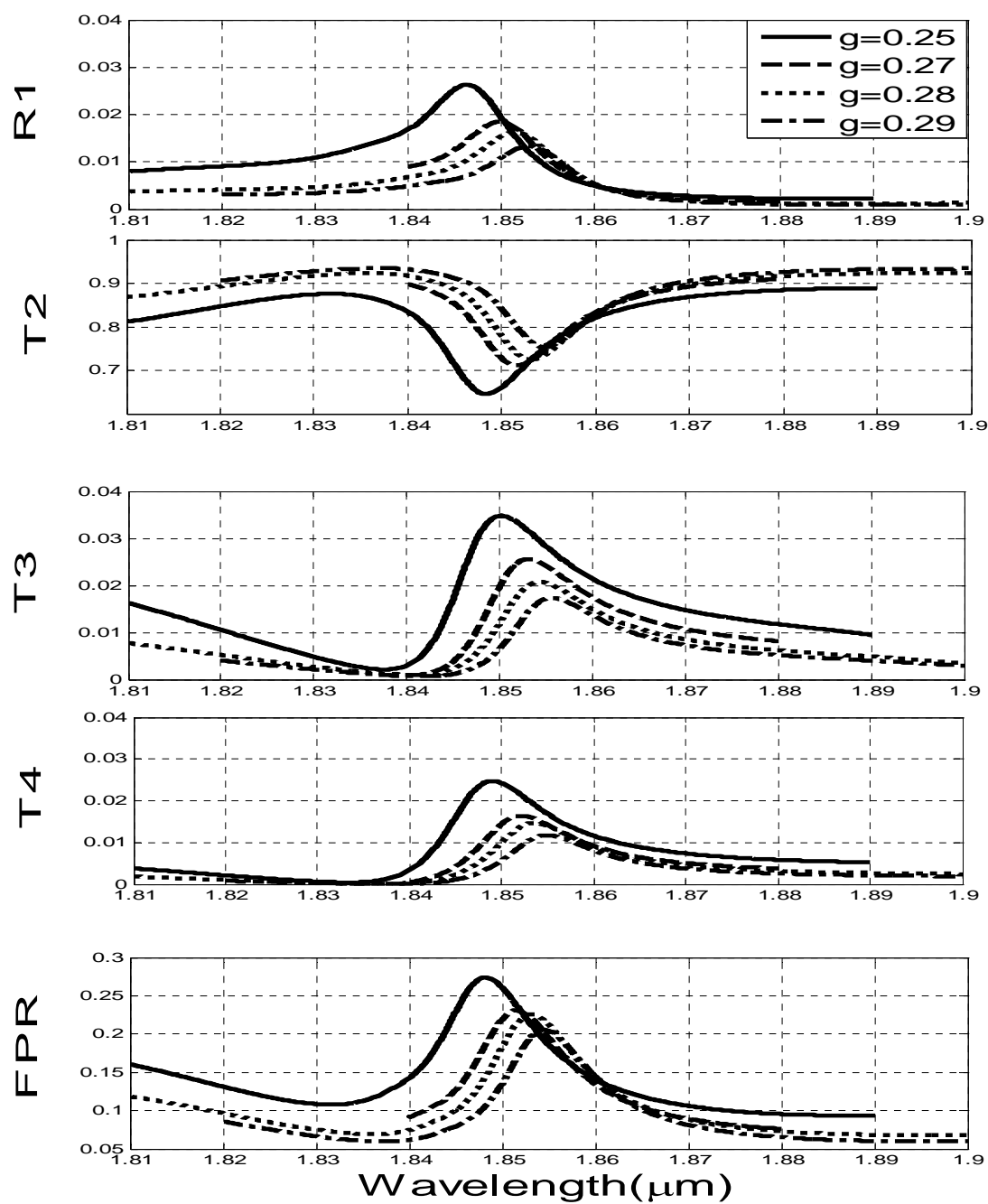
Figure 8.2: Spectral Response of Add/Drop Filter with Parallelogram Shaped Cavity for different Air Gaps.

Effect of the width w:

The height h and the air gap are fixed at 1.54μm and 0.27μm. The width w is varied from 1.50μm to 1.58μm and the effect of varying the width w on the spectral response of all the four ports is shown in figure 8.3. From this figure, it can be seen that as the width w is increased:

I. The resonant wavelength shifts towards higher wavelengths.

II. Reflection at the input port and transmission to the other three ports increases.

III. The fraction of power radiated increases.

Thus, we can see that for every 4μm change in the width w, the shift in the resonant wavelength is approximately equal to 0.02μm. The minimum modal reflectivity at port 1 increases from 0.0165 to 0.0192. The modal transmissivity at port 2 has a peak value of 0.74 at w= 1.50μm, and it decreases to 0.68 at w=1.58μm. The modal transmissivity at port 3 increases from 0.022 to 0.029. The peak value of the modal transmissivity at port 4 increases from 0.013 to 0.0202 as w increases from 1.50μm to 1.58μm. The fraction of power radiated increases from 0.22 to 0.25.
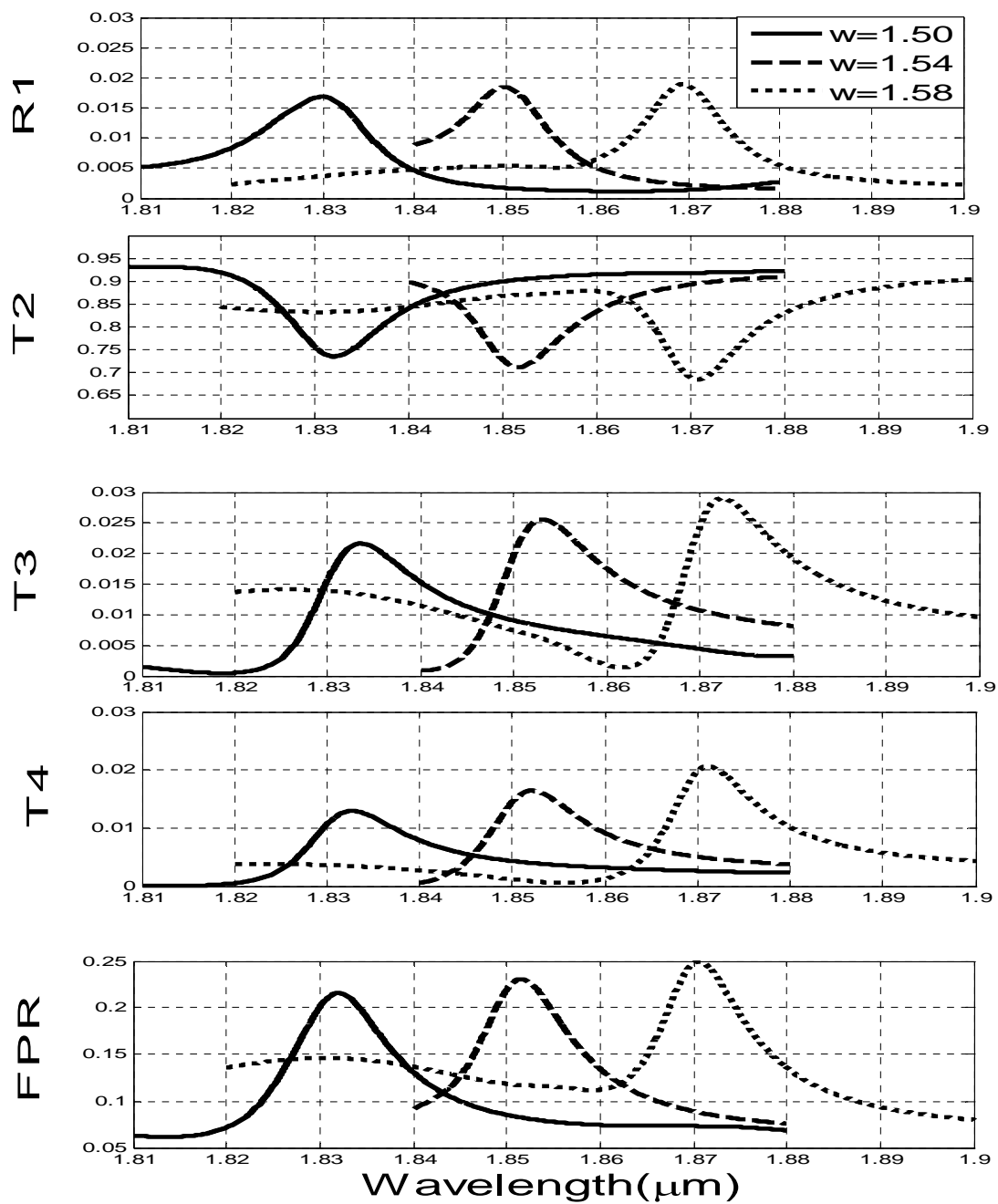
Figure 8.3: Spectral Response of Add/Drop Filter with Parallelogram Shaped Cavity for different Widths.

8.3 Add/Drop Filter with a Parallelogram Shaped Cavity Bent towards Right

A parallelogram shaped cavity bent towards right by an angle of 45° is placed between two parallel and identical waveguides as shown in figure 8.4. The width, height and the air gap are given by w, h and g, respectively.
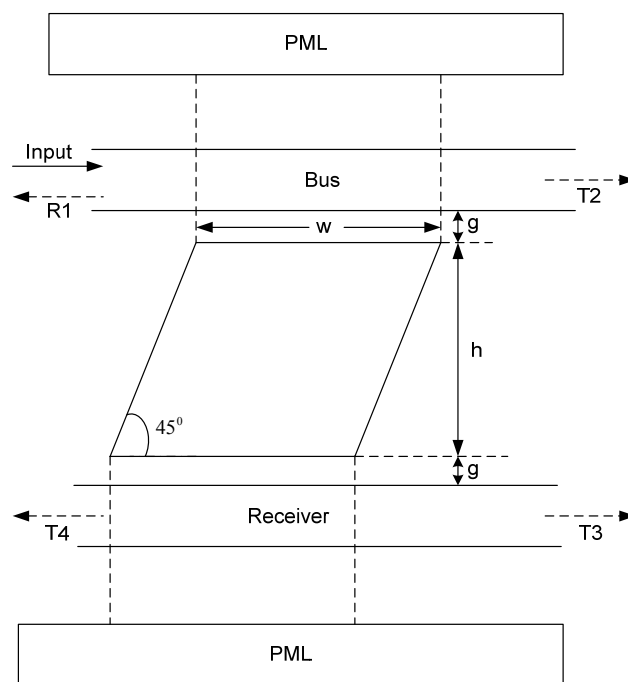
Figure 8.4: Add/Drop Filter with a Parallelogram Shaped Cavity Bent towards Right imbedded between Two Parallel Waveguides

8.3.1 Numerical Results for Add/Drop Filter with Parallelogram Shaped Cavity Bent towards Right

A parallelogram shaped cavity, bent towards right, is simulated using the MOL. The refractive indices, core widths and the mesh size are the same as considered in the previous cases. The height h, the width w and the air gap are fixed at 1.54μm, 1.54μm and 0.28μm respectively. Figure 8.5 shows a comparison between the spectral responses of all the four ports of the add/drop filters with parallelogram shaped cavities bent towards right and bent towards left. From this figure it can be seen that the resonant wavelength is approximately same for both the cases. The peak reflectivity at port 1, $R1$, increases from 0.0148 to 0.0151. Minimum modal transmissivity at port 2, $T2$, is reduced from 0.75 to 0.745. The modal transmissivity at port 3, $T3$, increases from 0.0069 to 0.0205 and the peak transmissivity at port 4, $T4$, increases from 0.013 to 0.0149. The peak value of the fraction of power radiated remains the same. Since the parallelogram shaped cavity is bent towards right side (see figure 8.4), the receiver is biased towards port 4 and shows clear discrimination of port 3. Although, the response of all the ports is maximum at a particular wavelength, but the response at other wavelengths is not completely zero. For an add/drop filter, the response of all the ports is maximum at a particular wavelength (i.e. the resonant wavelength) and the response must be zero at other wavelengths. Thus, we can conclude that a parallelogram shaped cavity placed between two parallel waveguides cannot be used as an add/drop filter. It can be used as a power splitter at a particular wavelength and has the advantage of being compact.
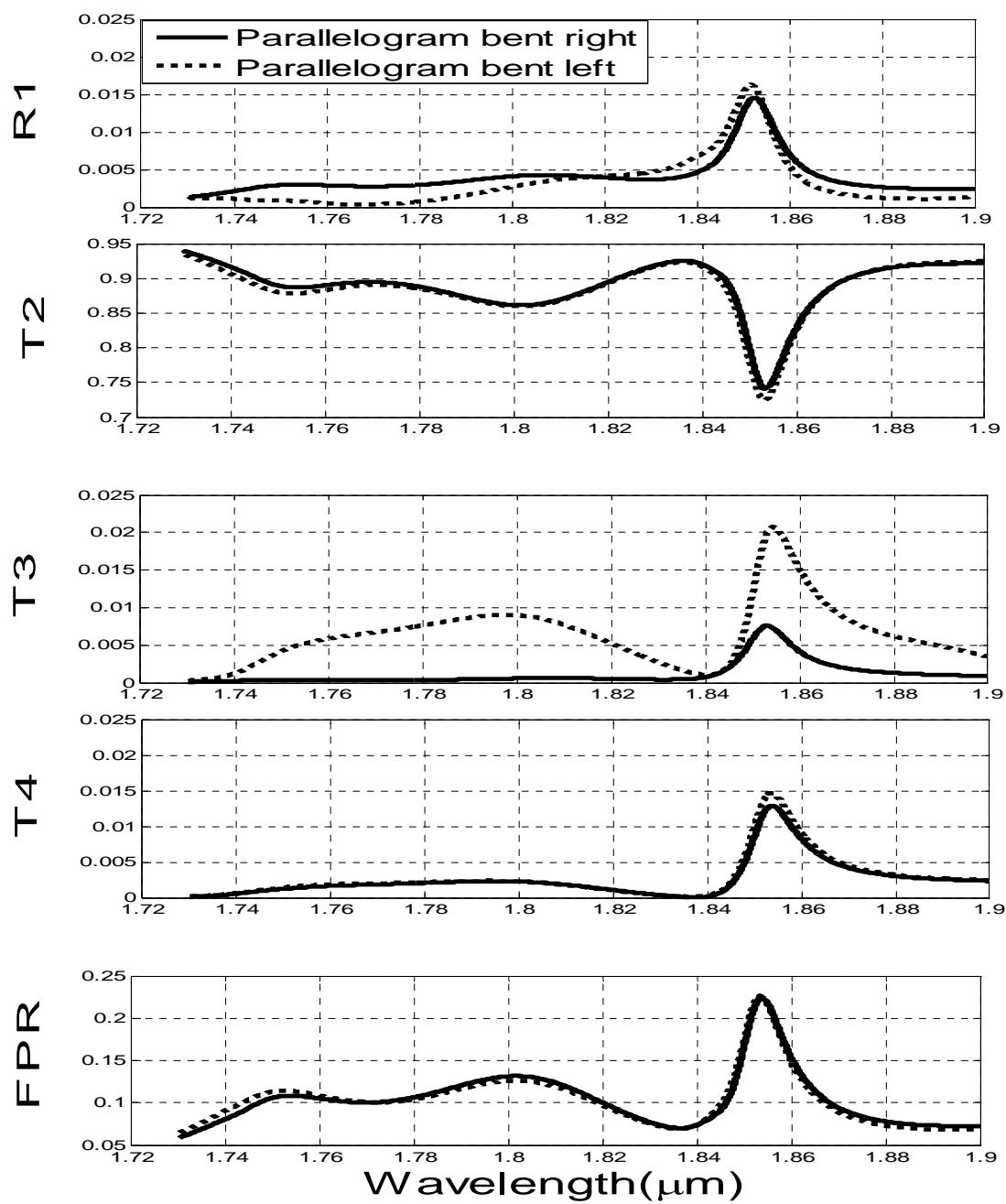
Figure 8.5: Comparison between Add/Drop Filters with Parallelogram Shaped Cavities Bent Towards Right and Towards Left.

Chapter 9

Summary, Conclusion and Future Work

9.1 Introduction

We have analyzed the filtering and coupling performance of add/drop filters imbedded with various planar cavity shapes. Both, the symmetric and asymmetric cavity shapes have been considered. The MOL using the Layer by Layer Algorithm has been applied to model these add/drop filters. In this chapter a brief summary of the work that has been carried out is presented. This is followed by conclusions and some suggestions for extension of the work which can be carried out.

9.2 Summary

A brief summary of the work done in this thesis work is listed below:

➢ A MOL code with three-point approximation of the transverse second order derivative operator has been developed.

➢ PML with absorbing boundary conditions with non uniform tangent loss profile has been incorporated into the MOL code and demonstrated. The PML has been used effectively throughout this work to absorb the radiative field.

➢ Longitudinal waveguide discontinuities have been studied using the MOL.

➢ The Layer by Layer Algorithm was incorporated into the MOL to analyze multiple longitudinal discontinuities. The MOL results were compared with results in the literature.

➢ Add/drop filters with imbedded square and rectangular cavities have been simulated with the MOL in tandem with the Layer by Layer Algorithm in an efficient manner. We have numerically calculated their spectral response on all four ports.

➢ The staircase approximation has been used efficiently with the Layer by Layer Algorithm in order to simulate add/drop filters with imbedded planar cavities. The cavities considered were the bow-tie, hexagon and parallelogram shaped cavities. The spectral response of all the four ports has been calculated numerically. We have also analyzed the effects of various parameters on the coupling and filtering performance of these add/drop filters.

9.3 Conclusions

> ➢ If the volume of a cavity placed between two waveguides and the air-gap increases, the resonant wavelength shifts towards higher wavelengths and vice-versa.

> ➢ The performance of add/drop filter improves with two identical Bow-tie shaped cavities compared to a single Bow-tie shaped cavity.

> ➢ An add/drop filter with Hexagon shaped cavity starts to lose its dropping capacity when the angle θ exceeds 3° or the cavity width w becomes less than 1.54µm.

> ➢ A parallelogram shaped cavity placed between two parallel waveguides cannot be used as an add/drop filter. It can be used as a power splitter and has the advantage of being compact and wavelength selectivity.

> ➢ It can be concluded that complete dropping from bus to receiver is not possible for an add/drop filter with a single planar cavity.

9.4 Future Prospects

The following is a brief list of suggestions for possible future works in this area:

> ➢ We have analyzed the spectral response of add/drop filters with single and double bow-tie shaped cavities, a rectangular, hexagonal and parallelogram shaped cavities. Multiple bow-tie, hexagonal and parallelogram shaped cavities can be used. It is expected that the

filter response and its capability to drop optical power from the bus to the receiver to improve with respect to the single and double cavity schemes.

➤ Analysis of an add/drop filter with an asymmetric cavity shape has been carried out using a parallelogram shaped cavity. Other asymmetric shapes can be investigated for the analysis of an add/drop filter.

➤ The developed MOL code can be improved in order to calculate the field intensity distributions inside the analyzed add/drop filters.

➤ All the numerical simulations done in this thesis work are for 2D models. An extension of this to 3D can also be done as 3D waveguide modeling gives more realistic results. Approaches like Pade approximations can be used for this purpose.

References

[1] S. E. Miller, *"Integrated Optics: an Introduction,"* Bell Syst. Tech. Journal, Vol. 48, PP.2059- 2069, 1969.

[2] S. E. Miller, "Light propagation in generalized lens like media," *Bell Syst. Tech. Journal,* Vol. 44, PP.2017-2064, 1965.

[3] H. Nishihara, M. Haruna and T. Suhara, *Optical Integrated circuits.* McGrawHill, 1989.

[4] A. Sharma, *"Collocation Method for Wave Propagation through Optical Waveguide Structures,"* Progress in Electromagnetic Research, (PIER) 11, Elsevier Science Publications Co., Inc., 1995 .

[5] C. R. Doerr*,* L. W. Stulz, D. S. Levy, L. Gomez, M. Cappuzzo, J. Bailey, R. Long, A. Wong-Foy, E. Laskowski, E. Chen, S. Patel, and T. Murphy, *"Eight-Wavelength Add–Drop Filter with*

True Reconfigurability," IEEE PHOTONICS TECHNOLOGY LETTERS, VOL. 15, NO. 1, JANUARY 2003.

[6] **R.** Germann, R. Beyeler, G.L. Bona, F. Horst, B.J. Offrein and H.W.M. Salemink, *"Wavelength-tunable add/drop filter for optical networks*," *IBM Research Division*, Zurich Research Laboratory, Saumerstr. 4.

[7] Min-Cheol Oh, Hyung-Jong Lee, Myung-Hyun Lee, Joo-Heon Ahn,Seon Gyu Hun, and Hue-Guen Kim*," Thermooptic Tunable Wavelength Filters Using Polymer Waveguide Bragg Gratings,"* Electronics and Telecommunications Research Institute.

[8] M. J. Khan, C. Manolatou, Shanhui Fan, Pierre R. Villeneuve, H. A. Haus and J. D. Joannopoulos, *"Mode-Coupling Analysis of Multipole Symmetric Resonant Add/Drop Filters," IEEE JOURNAL OF QUANTUM ELECTRONICS,* VOL. 35, NO. 10, OCTOBER 1999.

[9] *"Progress in High Index Contrast Integrated Optics,"* Ghent University-IMEC, INTEC Department, Photonic Research Group.

[10] Mohammad Mahbubul Islam. Analysis of add/drop optical waveguide filters with embedded resonant cavities using the method of lines. . Master's Thesis, King Fahd University of Petroleum and Minerals, Saudi Arabia, April 2005.

[11] Chung Yan Fong and Andrew W. Poon, "*Square μ -pillar cavity channel add/drop filters: FDTD simulation,K-space modeling and ray tracing*".

[12] Chung Yan Fong and Andrew W. Poon, "*Mode field patterns and preferential mode coupling in planar waveguide-coupled square microcavities*", Optical Society of America, 2003.

[13] Chung Yan Fong and Andrew W. Poon, "*Planar corner-cut square microcavities: ray optics and FDTD analysis*", Optical Society of America, 2004.

[14] Ning Ma, Chao Li and Andrew W. Poon, "*Laterally Coupled Hexagonal Micropillar Resonator Add-Drop Filters in Silicon Nitride*", IEEE Photonics tech. letters, vol. 16, No. 11, November 2004.

[15] K. R. Hiremath, R. Stoffer, M. Hammer, " *Modeling of circular integrated optical microresonators by 2-D frequency domain coupled mode theory*", MESA Institute of Nanotechnology, University of Twente, Enschede, The Netherlands, July 19, 2005.

[16] Damian Goldring, Uriel Levy, and David Mendlovic, "*Highly dispersive micro- ring resonator based on one-dimensional photonic crystal waveguide design and analysis*", Optical Society of America, 2007.

[17] B.E Little, S.T. Chu, W. Pan, D. Ripin, T. Kaneko, Y. Kokubun, and E. Ippen, " *Vertically coupled glass micro ring resonator channel dropping filters",* IEEE Photon. Technol. Letter 11, 215-217, 1999.

[18] Yih Peng Chiou and Hung Chun Chang. Analysis of optical waveguide discontinuities using pade approximation. *IEEE Photonics Technology Letters* 9:964-966, 1997.

[19] D. Benish J. Gerdes, B. Lunitz and R. Pregla. Analysis of slab waveguide discontinuities including radiation and absorption effects. *Electronics Letters,*28(11):1013, Mat 1992.

[20] J. Gerdes and R. Pregla. Beam-propagation algorithm based on the method of lines. *Optical Society of America (B),* 8(2):389-394, February 1991.

[21] Wei Dong Yang and R. Pregla. Method of lines for analysis of waveguide structures with multi-discontinuities. *Electronics Letters,* 31(11):892, May 1995.

[22] R. Pregla and W. Yang. Method of lines for analysis of multi-layered dielectric waveguides with bragg gratings. *Electronics Letters,* 29(22):1962, October 1993.

[23] R. Pregla and E. Ahlers. Method of lines for analysis of discontinuities in optical waveguides. *Electronics Letters,* 29(21):1845, October 1993.

[24] Abiodun Ahmad Shittu. *Study of periodic waveguides by the finite-difference time-domain method and the Method of Lines.* PhD thesis, King Fahad University of Petroleum and Minerals, Dhahran 31261, Saudi Arabia, September 1994.

[25] S. J. Al-Bader and H. A. Jamid. Method of lines applied to non-linear guided waves. *Electronics Letters,* 31(17):79-85, February 1995.

[26] M. Imtaar and S. J. Al-Bader. Analysis of diffraction from abruptly-terminated optical fibers by the method of lines. *Journal of Lightwave Technology,* 13(2):137-141, February 1995.

[27] J. Gerdes and R. Pregla. Beam-propagation algorithm based on the method of lines. *Optical Society of America (B),* 8(2):389-394, February 1991.

[28] Muhammad Nadeem Akram. Analysis of anti-resonant reflecting optical waveguide (ARROW) grating using the method of lines. Master's Thesis, King Fahd University of Petroleum and Minerals, Saudi Arabia, April 2000.

[29] H. Dietsel, Analysis of planar multi-conductor transmission line systems with the method of lines, Arch. Elektron Ueber, vol. 41, pp 169-175, 1987.

[30] H. Dietsel and S. Worm, Analysis of hybrid field problems by the method of lines with non-equidistant discretization, *IEEE Trans. Microwave Theory Tech.,* vol. MTT-32, no. 6, pp. 633-638, 1984.

[31] S. J. Al-Bader and H. A. Jamid. Perfectly matched layer absorbing boundary conditions for the method of lines modeling scheme. *IEEE Microwave and Guided Waves Letters,* 8(11):357-359, November 1998.

[32] H. A. Jamid. Frequency domain PML layer based on the complex mapping of space boundary condition treatment. *IEEE Microwave and Guided Waves Letters,* 10:356-358, September 2000.

[33] Mohammed Ameeruddin. Pade approximants technique for the analysis of waveguide junctions and beam splitters. . Master's Thesis, King Fahd University of Petroleum and Minerals, Saudi Arabia, May 2004.

[34] Y. P. Chiou and H. C. Chang. Analysis of optical waveguide discontinuities using pade approximation. *IEEE Photonics Technology Letters* 9:964-966, 1997.

[35] Wei Dong Yang and R. Pregla. Method of lines for analysis of waveguide structures with multi-discontinuities. *Electronics Letters,* 31(11):892, May 1995.

[36] R. Pregla and W. Yang. Method of lines for analysis of multi-layered dielectric waveguides with bragg gratings. *Electronics Letters,* 29(22):1962, October 1993.

[37] J. J. Gerdes, Bidirectional eigenmode propagation analysis of optical waveguides based on method of lines, Electronics letters, vol. 30, p. 550, March 1994.

[38] Q. – H. Liu and W. C. Chew, Analysis of discontinuities in planar dielectric waveguides: An eigenmode propagation method, *IEEE Transactions on Microwave Theory and Techniques,* vol.39, pp 422-430, March 1991.

[39] S. T. Peng and T. Tamir, TM mode perturbation analysis of dielectric gratings, *Applied Physics,* vol. 7, no. 35, pp. 35-38, 1975.

[40] Yih-Peng Chiou and Hung-chun Chang, "Analysis of Optical Waveguide Discontinuities Using the Pad´e Approximants", *IEEE PHOTONICS TECHNOLOGY LETTERS*, VOL. 9, NO. 7, JULY 1997.

[41] Alexander M. Kenis, Ilya Vorobeichik, Meir Orenstein, and Nimrod Moiseyev, "*Non-Evanescent Adiabatic Directional Coupler", IEEE Journal of Quantum Electronics,* vol.37 , No. 10, October 2001.

[42] Charles K. Kao, "Optical Fiber Systems: Technology, Design and Applications", McGraw-Hill, 1982.

[43] Abiodun Ahmad Shittu. *Study of periodic waveguides by the finite-difference time-domain method and the Method of Lines.* PhD thesis, King Fahad University of Petroleum and Minerals, Dhahran 31261, Saudi Arabia, September 1994.

[44] H. A. Jamid and M. N. Akram, "Analysis of deep waveguide gratings: an efficient Cascading and Doubling algorithm in the mrthod of lines frame work." *Journal of Lightwave technology,* 20(7):1204-1208, July 2002.

[45] J. Ctyroky, S. Helfert and R. Pregla, "Analysis of deep waveguide bragg gratings," *Optical and Quantum Electronics Letters,* vol. 14, pp.1533-1535, November 2002.

[46] C. Manolatou, M. J. Khan, Shanhui Fan, Pierre R. Villeneuve, H. A. Haus, *Life Fellow, IEEE* and J. D. Joannopoulos, " Coupling of Modes Analysis of Resonant Channel Add/Drop Filters," *IEEE Journal of Quantum Electronics,* vol. 35, No. 9, Sep. 1999.

Vitae

1983: Born in Hyderabad, India.

2006-2008: Master of Science in Electrical Engineering from King Fahd University of Petroleum

    & Minerals, Dhahran, KSA.

      ➢ Major: Integrated Optics.

2001-2005: B.E. Electronics and Communications Engineering at Osmania University,

    Hyderabad, India.

      ➢ First Division with Distinction.

2001: Distinction in Intermediate (Class 12), Little Flower Junior College, Hyderabad, India.

1999: Matriculation with Science Major at International Indian School, Dammam, KSA.